6-10-2020

Fabrication and characterization of polycaprolactone-based nanofibrous scaffolds for neuronal tissue regeneration

Manar Ahmed Elnaggar
The American University in Cairo

Fabrication and Characterization of Polycaprolactone-Based Nanofibrous Scaffolds for Neuronal Tissue Regeneration

Manar Ahmed El-Naggar

B.Sc. in Pharmaceutical Sciences

Submitted in partial fulfilment of the requirements for the degree of
Master of Science in Nanotechnology

School of Sciences and Engineering
The American University in Cairo
2020

`

Keywords

Regenerative Medicine, Electrospinning, Nanofibers, Fibronectin, Laminin, RGD, Neuronal Regeneration, Spinal Cord Injury.

`

Abstract

Recent advances in regenerative medicine have given hope in overcoming and rehabilitating complex medical conditions. In this regard, biomaterial scaffolds are employed to support cellular adhesion, elongation, and growth, thus promoting sound healing and restoration of function after trauma. The biopolymer poly-ε-caprolactone (PCL) may be a promising candidate for tissue regeneration, in this regard, although lacking essential bioactivity. The present study used PCL nanofibers (NFs) scaffold decorated with the extracellular matrix proteins fibronectin and laminin for neuronal regeneration. The potential for the combined proteins to support neuronal cells and promote axonal growth was investigated. Two NFs scaffolds were produced with concentrations of PCL: 12% or 15%. Under scanning electron microscopy, both scaffolds evidenced uniform diameter distribution in the range of 358 nm and 887 nm, respectively, and greater than 80% porosity. The Brunauer–Emmett–Teller test confirmed that the fabricated NFs mats had a high surface area, especially for the 12% NFs with 652 m^2/g compared to 254 m^2/g for the 15% NFs. Therefore, the 12% NFs was selected for further study. The proteins of interest were successfully conjugated to the PCL scaffold through chemical carbodiimide reaction as confirmed by Fourier-transform infrared spectroscopy. Moreover, the in-vitro degradation test showed slow degradation rate. The addition of fibronectin and laminin together was shown to be the most favorable for cellular attachment and elongation of neuroblastoma SH-SY5Y cells. Confocal light microscopy revealed longer neurite outgrowth, higher cellular projected area, and lower shape index for the cells cultured on the combined proteins conjugated fibers, indicating enhanced cellular spread on the scaffold. This preliminary study suggests that PCL scaffolding conjugated with matrix proteins can support neuronal cell viability and neurite growth, suggesting potential application in cases of spinal cord injury (SCI).

`

Table of Contents

`

`

`

List of Figures

`

`

List of Tables

`

List of Abbreviations

ASCs	activated Schwann Cells
CA	Citric Acid
ChABC	Chondroitinase ABC
CNS	Central Nervous System
DMSO	Dimethylsulfoxide
ECM	Extracellular Matrix
FBN	Fibronectin
FBS	Fetal Bovine Serum
FESEM	Field Emission Scanning Electron Microscope
FTIR	Fourier transform-Infra red spectroscopy
GDNF	Glial cell-Derived Neurotrophic Factor
hNP-ACs	human Neural Progenitor-derived Astrocytes
iPSC	induced Pluripotent Stem Cells
ISCOS	International Spinal Cord Society
LAM	Laminin
MAG	Myelin-Associated Glycoprotein
MENA	Middle East and North Africa
MTT	(3-(4, 5-Dimethylthiazol-2-yl)-2, 5-Diphenyltetrazolium Bromide)
NFs	Nanofibers
NGF	Nerve Growth Factor
NSCs	Neural Stem Cells
NT3	Neurotrophin 3
OMgp	Oligodendrocyte Myelin glycoprotein
OPC	Oligodendrocyte Progenitor Cells
PANI	Polyaniline
PBS	Phosphate Buffer Saline
PCL	Poly-Caprolactone

`

PLGA	Polylactic-co-glycolic Acid
PNI	Peripheral Nerve Injury
PSA	Polysialic acid
RGD	Arginylglycylaspartic acid
RPMI-1640	Roswell Park Memorial Institute Medium
SAMs	Self-Assembled Monolayers
SCI	Spinal Cord Injuries
SH-SY5Y	Neuroblastoma
SP	Spinal Cord
WHO	World Health Organization

`

Statement of Original Authorship

The work encompassed in this thesis has not been submitted in prior to fulfill requirements of any degree or award at the American University in Cairo or any other research institution. I certify, at the best of my knowledge, that this thesis does not contain material written or published by other persons unless the work referred to.

Signature: Manar Ahmed ElNaggar

Date: June 4th, 2020

`

Acknowledgements

First, I would like to address my deep gratitude to my thesis advisors; Dr. Nageh Allam and Dr. Hassan El-Fawal for their continuous guidance and support during the whole period of my study and research. Their constructive feedback enriched the work that has been done and enabled a sound development of the different parts of this research.

Also, I would like to thank the moderator Dr. Anwar Abdel-Nasser and the examiners Dr. Mohamed Salama and Dr. who took part in the reviewing and verification of this thesis project, and I am enormously grateful for their appreciable comments on this thesis.

I would like to extend my gratitude to Al-Ghurair Foundation for Education and Allehdan scholarship for funding my study at AUC. This work was financially supported by the American University in Cairo. I would like also to thank to Dr. Shahenda Elnaggar from 57357 hospital for providing us with the neuroblastoma cell line and to my dear friend Diana Sami who provided me with different needed materials and more importantly, helped me with her expertise. And to all my team in helping me and giving me required trainings to get ready for experimental work: Marwan Yasser helped me with the electrospinning process, Alaa Hamed and Omneya Mahmoud helped me in learning cell culture techniques. Special thanks to Nashaat Ahmed, Amina Saleh, Islam Mamdouh, Manar Hazaa, and Doha Sayed for their help in different part of the chemical or physical characterization.

Finally, I would like to express my profound appreciation and gratitude to my parents, brothers; Maher and Adel, and friends; Amal, Sherif, Yousof, Sarah, Osman, for their unconditional support and ceaseless encouragement. I would not have been able to accomplish my degree without their love and compassion. Thank you.

1. Introduction

1.1. Neural Tissue Injury: Spinal Cord and Medical Complications

The brain and spinal cord (SC) constitute the Central Nervous System (CNS)[1,2]. Injuries to the SC affect motor, sensory and autonomic functions, leading to deleterious health, social and economic impact. This includes decreased school attendance, disabled work-social life and lower self-esteem[3–6]. According to the World Health Organization (WHO) and the International Spinal Cord Society (ISCOS), the global prevalence of Spinal Cord Injuries (SCI) varies from 1048 to 2528 per million population, with incidence that ranges from 40 to 80 new incidents per million population annually[3]. This rate varies from one country to another, as in the United States (US), the National Spinal Cord Injury Statistical Center in Alabama reported 54 cases per million people[5]. In the MENA region, a meta-analysis done in Mansoura University indicated an incidence rate ranging from 6 to 50 cases per million people annually[7]. It is worth noting that reported statistics vary widely and more research is needed to get accurate global prevalence and incidence of SCI[5]. Despite reported lower incidence of SCI in developing countries compared to developed countries[8], secondary complications and mortality rate rank above global average in low/middle income countries due to limitations in healthcare centers capable of managing SCI[3,8]. The major cause of SCI globally is traffic accidents, followed by falls and violence[3,4,8]. In some places, falls account as the leading cause of SCI, as in Finland[9], Latvia[10], Nepal, Pakistan and Bangladesh[8]. Regardless of cause, SCI has major impact acutely and chronically, affecting mostly the young adult males in their twenties and thirties[3,4,7,8,10,11]. Studies also indicate the predominance of complete paraplegia over incomplete injuries[7] or tetraplegia[7,8]. Unfortunately, people suffering

`

SCI are more prone to premature death at two to five times the rate of healthy counterparts[3,9] , with high fatality rate during first year[3,4], which may reach up to 13% in US[4].

The lifetime management of SCI requires considerable healthcare resources and places a significant financial load, not only on the patients, but on the whole community, especially if the injury makes the victim rely on assisted daily care to aid them in overcoming physical hurdles in communication and mobility. For example, a single case of SCI in US in 1997 cost 0.5 to 2 million USD according to the case severity and location of the injury[12], this number increased to 1.1 to 4.6 million USD[3] in 2013 and then again to 1.2 to 5 million USD[13] in 2018. Overall, the total annual -direct- cost on the overall American health system was estimated to be 4 billion USD in 1990[4] and increased to 7.7 billion USD in 1997[12]. In Canada, 2013, the lifetime cost per case was estimated to range from 1.5 to 3 million Canadian dollars. And the total healthcare expenditure for new incidents annually was 2.67 billion Canadian dollars[14]. Another example in Australia, 2009, the estimated total healthcare costs ranged from 52.5 to 76.5 million Australian dollars[15]. Also, in the Netherlands, 1999, SCI management costed 1.15 billion-euro, equivalent to 3.7% of total health expenditure of the country at that time[16]. Generally, healthcare costs are the highest during first year of trauma, then tend to decrease significantly onward[3,15]. Adding to all of this, the uncalculated -indirect- costs due to productivity and income loss should be also considered[4], which in some cases exceed the direct costs of the treatment[3]. These indirect costs were estimated in US, 2018, to be around 70K USD annually per case[13].

`

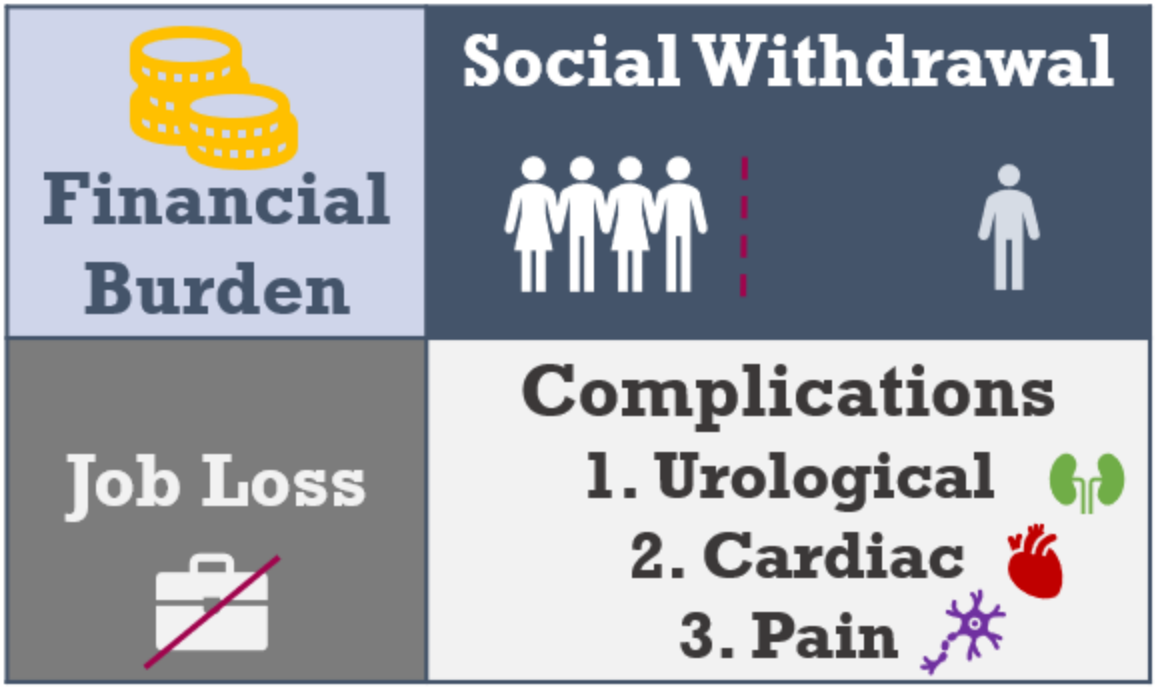

Figure 1. Multiple consequences of SCI.

The popular conception of SCI revolves around the paralysis and the restriction of hand and / or leg movement. However, victims of SCI suffer heavily from other lifelong complications that might be more life determining than affected movement. Among which, pulmonary complications, cardiovascular disorders, pressure ulcers[11,17], urological complications[17], loss of bowel and bladder control, spasticity, nociceptive and neuropathic pain, sexual dysfunction and heterotopic ossification[3,6,18,19]. The overall clinical situation after SCI is highly affected by the site of injury[6], **Figure 1**.

1.2. Limitation of Medical Intervention in SCI

To understand the limitations of treating SCI, it is necessary to identify the changes that take place when the SC is impaired. After an injury, the spinal cord, or parts thereof, gets severed immediately due to the mechanical impact of the trauma, known as primary injury, and the

`

secondary pathological process occurring at the site of injury, known as secondary injury[6,12]. Clinically, SCI is classified to acute, within 2 to 48 hours of the injury, subacute, within 2 days to 2 weeks, the intermediate, within 2 weeks to 6 months, and chronic, occurring more than 6 months of the injury onset[2,6].

Primary injury results from the compression or contusion of the spinal cord by the fracture and displaced vertebral bones, and its magnitude depends on the energy transferred to the tissue from the primary impact[2]. This results in disruption of the blood vessels supplying the spinal cord and damage of the neuronal cell membrane[2,4,6,12]. Within few minutes to few hours of the onset of the injury, secondary injury cascade is initiated. Neurogenic shock starts developing as microhemorrhage takes place at the injury site, and spinal cord swells, leading to ischemia[2,12]. Hypotension and bradycardia then follow the neurogenic shock, worsening ischemia and release of toxins, cell suicide and death of neighboring neurons[6,12]. Neurogenic shock intensity is more severe in injuries affecting spinal cord above T6 vertebra, this is due to the imbalanced autonomic control and weakened sympathetic stimulation compared to the vagal tone, leading to prominent bradycardia and hypotension[2,6]. Secondary injury severity depends mainly on the primary injury impact. It is known as a cascade of biochemical and cellular events, regulated through a feedback loop, leading to disturbance of the microenvironment surrounding the neuronal tissue at the site of trauma[2,4,6]. Along with the vascular disturbance, there is an over secretion of neurotransmitters like glutamate, catecholamine and serotonin accumulate, all of which surge the excitability of adjacent spared neurons. Glutamate-mediated excitotoxicity, in particular, is involved in white matter damage, an effect that continues to take place for days after initial injury. This may lead to oligodendrocyte death and demyelination, affecting not only severed neurons, but also affecting

`

healthy neurons [12,20–22]. In addition, glutamate over-stimulates adjacent neurons, which in turn increases intracellular calcium and extracellular potassium[4,12]. Increased Ca^{++} concentration activates Ca^{++} -mediated proteases, nitric oxide synthetase with ensuing release of highly reactive free radicals which interacts with membrane lipids causing their peroxidation, membrane destruction and cell death[2,12].

As self-clearance mechanism, the body initiate inflammatory reaction to remove cellular debris. Briefly, within few minutes of the injury, astrocytes and microglia, which are major non-neuronal component of CNS with variable phagocytic ability, send chemical signals to recruit blood-borne cells responsible for clearance, like meningeal fibroblasts, pericytes, perivascular fibroblast-derived stromal cells and other immunologic cells including macrophages, neutrophils and lymphocytes[23,24]. Different types of macrophages are activated in a desynchronized pattern, which hinders wound healing[25]. All these accumulating cells then reside in the lesion core [24]. Scarring may begin as early as 48 hours and up to a week following insult. The forming scar is an attempt to isolate the injury and to protect adjacent cells. Newly proliferated local astrocytes are mainly involved in the scar formation process in a process of reactive astrogliosis[23], along with reactive oligodendrocyte progenitor cells (OPC) producing chondroitin sulphate proteoglycans that inhibit axonal regeneration[22,24]. All of this ultimately lead to Wallerian degeneration of the axon[26].

It should be noted that there may be some spontaneous functional recovery after SCI manifested in spontaneous regenerative and compensatory sprouting in unlesioned descending tracts and which may be associated with partial functional recovery. In addition, network reorganization may occur through synaptic adaptation in spinal circuits patterns[26]. However, this

`

natural sprouting is short distanced for 0.2 to 2 mm and is inhibited by the inflammatory microenvironment at the injury site[26].

1.3. State of Therapeutic Intervention

The combination of delineated events poses a challenge that limits axonal regeneration after SCI. Different management approaches, with variable success, exist for the various cases of SCI. This includes surgical intervention, administration of pharmacological and biological agents, neuromodulation and electrical stimulation, rehabilitation and, most recently, regenerative medical techniques. Unfortunately, many of these modalities succeed only in stabilization of secondary injury[12,26]. Furthermore, the majority of these interventions remain under investigations.

Surgical Intervention. SCI may need surgical intervention, known as early decompression, especially in case of compression or neurological deficiency and within the first 24-hours after injury or maybe later[6,27]. The aim of the surgery is to immobilize the spine in place and to restore its original alignment, and to remove any sort of compression, like bony structures, to preserve neurological functions as much as possible. In cases where vertebrae are broken, surgeons may insert hardware or transplanted bone to allow fusion. The spine is supported using a brace or other stabilization devices until the patient is mobile[6,12].

Intervention using Pharmacologic and Biological Agents. Currently pharmacological intervention is limited to symptomatic correction of neurogenic shock, hypotension or other functional complications. Furthermore, the use of methylprednisolone or other anti-inflammatory corticosteroids is controversial and thus not recommended for acute management[27].

`

Currently, there are some ongoing pre- and clinical trial of some pharmacological and biological agents that aims to protect the axon. One of the currently studied treatment approaches is intrathecal injection of the bacterial enzyme Chondroitinase ABC (ChABC) at the injury site[12,26,28–31]. Moon *et al.*, 2001[30,31], found that ChABC is responsible for the digestion of chondroitin sulphate proteoglycans that develop in the glial scar's extracellular matrix (ECM) at the site of injury. These proteoglycans inhibit axonal growth and thus, their degradation, hypothetically, allows sprouting of neuronal regeneration and axon elongation. Conducted *in-vivo* studies indicated significant functional and electrophysiological recovery, although anatomical recovery was limited[30–32]. Building on these promising results, in 2011, Wang *et al*[28]. examined the combinatorial effect of chondroitinase ABC with task-specific rehabilitation exercises four weeks after cervical SCI to mimic chronic injury in Male Lister hooded rats. They found paw reaching recovery and improvement in ladder and beam walking, however, this high gain was not sustained[28]. Recently in 2018, double-blinded randomized controlled trial have been conducted in 60 dogs for heat-stabilized, lipid microtube-embedded chondroitinase ABC intraspinal injection. Treatment and its duration both affected the suffering dogs. After a 6-month follow-up of chondroitinase-treated animals, a mean of 23% improvement in coordination between forelimbs and hindlimbs was achieved. Also, three dogs (10%) in the chondroitinase group recovered the ability to ambulate without assistance. On the other hand, there was neither improvement of bladder compliance, nor overall differences between groups in detection of sensory-evoked potentials[29,33].

Another treatment modality that is being studied is the blockade of myelin-associated growth inhibitors like Nogo-A[32,34], oligodendrocyte myelin glycoprotein (OMgp) and myelin-

`

associated glycoprotein (MAG)[22,26,35,36]. In normal conditions, Nogo-A is a transmembrane protein, expressed by oligodendrocytes[26,36]. Nogo-A is responsible for the stabilization of synapses and controlling neuronal plasticity, learning and memory[34,36]. However, in case of SCI, Nogo-A binds to complex receptor and is internalized within the cell, activating intracellular Ca^{2+} pathways Rho A and ROCK, affecting the actin and integrin stability within the growth cones and leading to their collapse[26,34]. Also, Nogo-A inhibits activation of mTOR growth regulator[34]. *In-vivo* animal studies on rats using anti-Nogo-A antibodies resulted in long distance axonal regeneration and improved locomotion[37], in addition to increased descending serotonergic fibers density[38]. Interestingly, Wang *et al.* demonstrated equivalent results in delayed (after three days of injury onset) anti-Nogo-A treatment using (NgR(310)ecto-Fc) fusion protein compared to acute intervention[39]. Other studies have been carried on macaque monkeys reporting recovery of hand function[40]. Successfully, a phase I clinical trial was conducted late 2006 and ended 2011, to test the effect of intrathecal injection of ATI 355 anti-Nogo-A antibody within 4 to 14 days of injury onset, with acute, complete traumatic paraplegia and tetraplegia SCI in humans. The study resulted in tolerated treatment for 52 cases without significant signs of side effects[26,41,42]. Recently, a phase II clinical trial, NISCI (Nogo-A Inhibition in acute Spinal Cord Injury), was launched in Switzerlandusing NG-101 anti-Nogo-A antibody within 4 to 28 days following incomplete SCI, and is projected to enroll 132 participants and to continue into late 2023[43].

Neuromodulation. This treatment modality encompasses electrical and magnetic stimulation to stimulate rewiring of neuronal circuits and trigger cells activity. This is accomplished by inserting a pacemaker-like device, responsible for firing electrical signals into the spinal cord. Electrical stimulation amplifies inbuilt sensory feedback and central pattern

`

regeneration in spinal cord with minimal supraspinal control[44]. Also, neuromodulation is widely used for the management of chronic spinal pain frequently occurring after SCI, although many patients may develop tolerance to the effect of stimulation overtime[45]. The most commonly used devices are epidural stimulators which researchers believe work through the activation of motor neurons located in posterior roots of spinal cord[46,47]. Epidural devices are invasive, whereas transcutaneous implants showed similar responses while being less invasive[46]. The major challenge for the development of effective neuromodulation devices is that the mechanism of their action is not fully understood[48]. To this end, closed-loop stimulations have been employed, where the spinal stimulator sends and receives signals. These signals are analyzed in a real-time technique by computational method to recognize and adapt the best pattern of movement stimulation that results in optimum recovery. Interestingly, some researchers have reported that the timing, place, and magnitude of the stimulation relative to muscle contraction/relaxation are important factors affecting axonal plasticity and recovery during treatment[47,49]. Currently, there is an ongoing randomized clinical trial to compare the effect of bilateral sacral stimulation for S3 nerve roots versus standard neurogenic care in the restoration of bladder function during first three months of the onset of SCI. The trial includes 60 patients and expected to end in September 2020[50].

Rehabilitation. Rehabilitation is an integral part of SCI management that aims to help patients to resume essential daily life activity with minimal dependence. It is a long and slow process and usually combined with other treatment modalities. The rehabilitation plan consists of a bundle of trainings and exercises that are tailored for each case, in acute and chronic onset, with targeted functional recovery[51]. It starts as early as possible with stretching exercises to manage flaccid muscles during the neurogenic shock[51,52]. Physical therapists train patients to accomplish

`

bowel programs, to self-catheterize and to utilize assistance devices including wheelchairs, walkers, and orthoses. Further, gait training is performed, and it could be either robotic-assisted gait training or body weight supported treadmill training. In addition, there are external battery-powered devices designed to support the limbs during various kind of movement[51–53].

1.4. Regenerative Medical Approaches

Regenerative medicine is an interdisciplinary field that combines various life science principles and technology with application to tissue healing and the restoration of lost function. Regenerative medicine uses multiple approaches, including the fabrication of scaffolds of biomaterial to mimic the natural tissue environment, delivery of cells and/or biopharmaceuticals products. Several of these have been studied in cases of SCI[54], **Figure 2**.

`

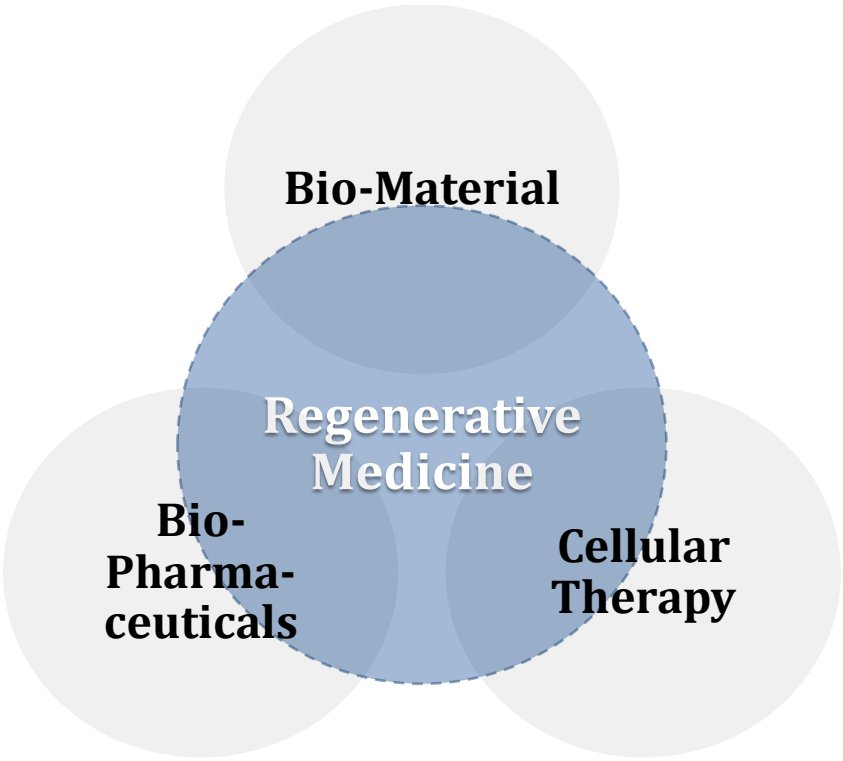

Figure 2. Cornerstones of regenerative medicine: biomaterials, cellular therapy, and biopharmaceuticals.

Currently, the development of new biomaterials exhibiting biological and/or pharmacological activity for tissue regeneration is being actively investigated to promote the growth of healthy tissue after different traumas[55,56]. This is a major challenge specially in cases of limited physical and functional recovery such as for SCI[57].

Recently, some clinical trials were approved to examine the use of biomedical scaffolds in SCI patients. The first study, INSPIRE, started in 2014 and expected to end 2024. Toselli and his group are examining bioresorbable poly(lactic-co-glycolic acid)-b-poly(L-lysine) cylindrical scaffold in subjects with thoracic level A (the most severe) traumatic SCI (T2-T12 level). The study was non-randomized, single armed with no control or comparison group, and the primary preliminary result published showed an overall 44% enhancement[58]. Meanwhile in 2019, the same

`

group started another investigation using the same scaffold, INSPIRE II, where the study is randomized and controlled with parallel assignment[59]. Another team lead by Jianwu Dai conducted two clinical studies investigating the transplantation of a functional collagen scaffold in acute SCI. The first one is a single armed study that started in 2015 and expected to end by 2020[60]. While the second trial started 2019 and investigates the combined effect of epidural electrical stimulation[61].

In the following section, over the focus is an overview of relevant literature regarding the technology, electrospinning, and applications being investigated using polycaprolactone NFs for neuronal regeneration, in general, and especially after SCI.

`

2. Nanotechnology in Regenerative Medicine

2.1. Electrospun Fibers in Tissue Regeneration

Electrospinning is one of the widely used techniques to fabricate polymeric fibrous scaffolds with individual fiber diameter ranging from the micro- to the nanoscale. In the electrospinning technique, high voltage is applied to draw a polymeric solution from a nozzle to the surface of a collector, **Figure 3**. The first drop formed at the tip of the nozzle is called "Taylor cone". When the applied voltage surpasses the surface tension of this Taylor cone, the droplets of the solution acquire charges that causes repulsion forces and causes spraying of the polymer. The polymeric solution at adequate viscosity allows the transformation of long fiber threads of polymer instead of showering droplets of the solution[62,63].

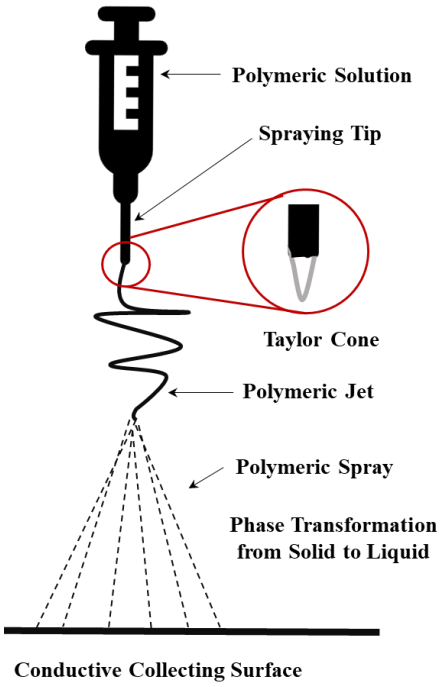

Figure 3. Electrospinning setup.

`

The electrospinning is considered a well-established and efficient technique, especially for scaling up. There are multiple parameters that are carefully controlled in order to achieve the desired characteristics and geometry of the scaffold, including the composition of the polymeric solution, the orifice size of the nozzle, the pumping pressure of the solution, the voltage of electric power, the collector style either rotating or static and the distance between the nozzle and the collector[56,64].

NFs, as bio-scaffolds, are considered a cornerstone in regenerative medicine and tissue engineering. They act as physical support that mimic extracellular matrix, support tissues and aid their repair and growth through adhesion[63]. In the last twenty years, NFs platforms have increasingly caught the interest of the regenerative medicine community for its various potential applications in the treatment of different medical conditions, **Figure 4**.

`

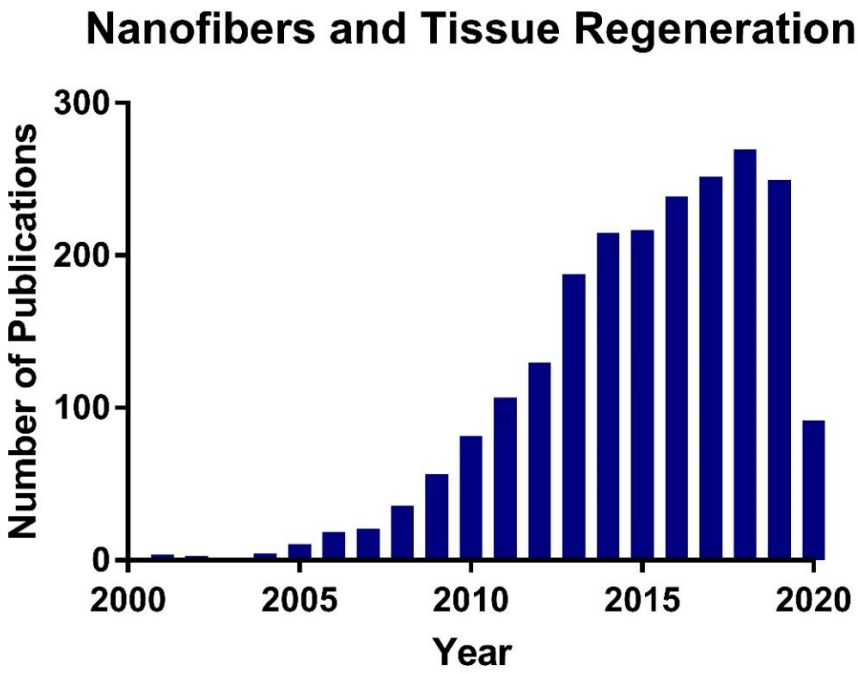

Figure 4. Yearly rate of publications related to the application of NFs in tissue regeneration over last twenty years[65]**.**

The shape and size of the NFs are more like the natural extracellular matrix which is mainly composed of collagen of diameter between 50 to 500 nm[66]. Nanostructures of fibrous scaffolds stimulate growth cones of neurons by providing bio-mechanical cues that trigger haptotaxis[67]. There are many considerations that must be accounted for while designing a successful nanofibrous scaffold, especially for neuronal grafting. First, the scaffold has to be biocompatible regardless of the target tissue for repair, it should not trigger immunological responses in the host tissue chronically, and if it degrades, biodegradation products should also be non-toxic[68]. Usually optimum degradation rate should be equivalent to tissue regeneration rate to allow optimum contact time with scaffold, while degrading upon tissue healing to accommodate tissue growth, which takes months at least from three to six months in cases of central nervous system repair[69,70].

`

There are other parameters including the pore size and density, flexibility, surface roughness, and mechanical strength of the scaffold[71]. In addition to their main role in supporting tissue regeneration, nanofibrous scaffolds could be functionalized to enhance scaffold-cells interaction. They also may be drug loaded with bio-pharmaceutical agents and growth factors to adjust for unbalanced microenvironment and to maximize drugs efficiency, thus improving the healing process. Interestingly, successful nanoscaffolds in cases of SCI can spare the use of autografts of peripheral nerves , as this approach has shown limited efficiency[72].

Polymeric NFs hold great promise as they can be designed and manipulated chemically, physically, and biologically to satisfy the specific needs for neuronal injuries. First of all, polymers are characterized by carbon-based chemistry, making them more appealing to biological tissues than other inorganic materials[73]. Particularly, synthetic polymers are preferred in tissue regeneration over natural polymers as they are more reproducible and more stable against environmental conditions. Also, if they degrade in-vivo, their by-products do not vary from patient to patient. In addition, synthetic polymers are less triggering for immunological reactions than natural products[73,74]. However, synthetic polymers lack the complex structure of natural polymers, which is desirable for specific in-vivo cellular interaction. For this reason, introducing biologically active functional group into the synthetic polymers has been employed to overcome their restricted bioactivity, such as using blends of synthetic and natural polymers, fabrication of co-polymers, or surface modification[73].

2.2. Polycaprolactone Biomaterial

Poly-ε-caprolactone (PCL) is an inert and biocompatible polymer with attractive mechanical properties and desired degradation rate[75–77]. PCL is a linear aliphatic semicrystalline

`

polyester[78]. It is hydrophobic and flexible biopolymer that has been employed in various tissue engineering applications[75,76,78]. The used molecular weight of PCL for electrospinning is uasually 80,000 Dalton, as smaller molecular weight does not produce polymeric solution with adequate viscosity for electrospinning and has low elasticity. Even though the most widely used solvent employed in the electrospinning of PCL was chloroform, many other solvent systems can be used including methanol, absolute acetic acid and formic acid[77]. Also, it is successfully electrospun in combination with various polymers, like chitosan, gelatin, polylactic acid, and others[77].

For example, Zhou *et al.* [78] fabricated random PCL NFs seeded with stem cells and neural derived stem cells, **Figure 5**. Complete physicochemical characterization for the scaffold was not done, yet the in-vivo transplantation of this scaffold resulted in an increased expression of Glial cell-Derived Neurotrophic Factor (GDNF) and Nerve Growth Factor (NGF) with a resulting improvement in locomotor activity compared to the control group[79].

`

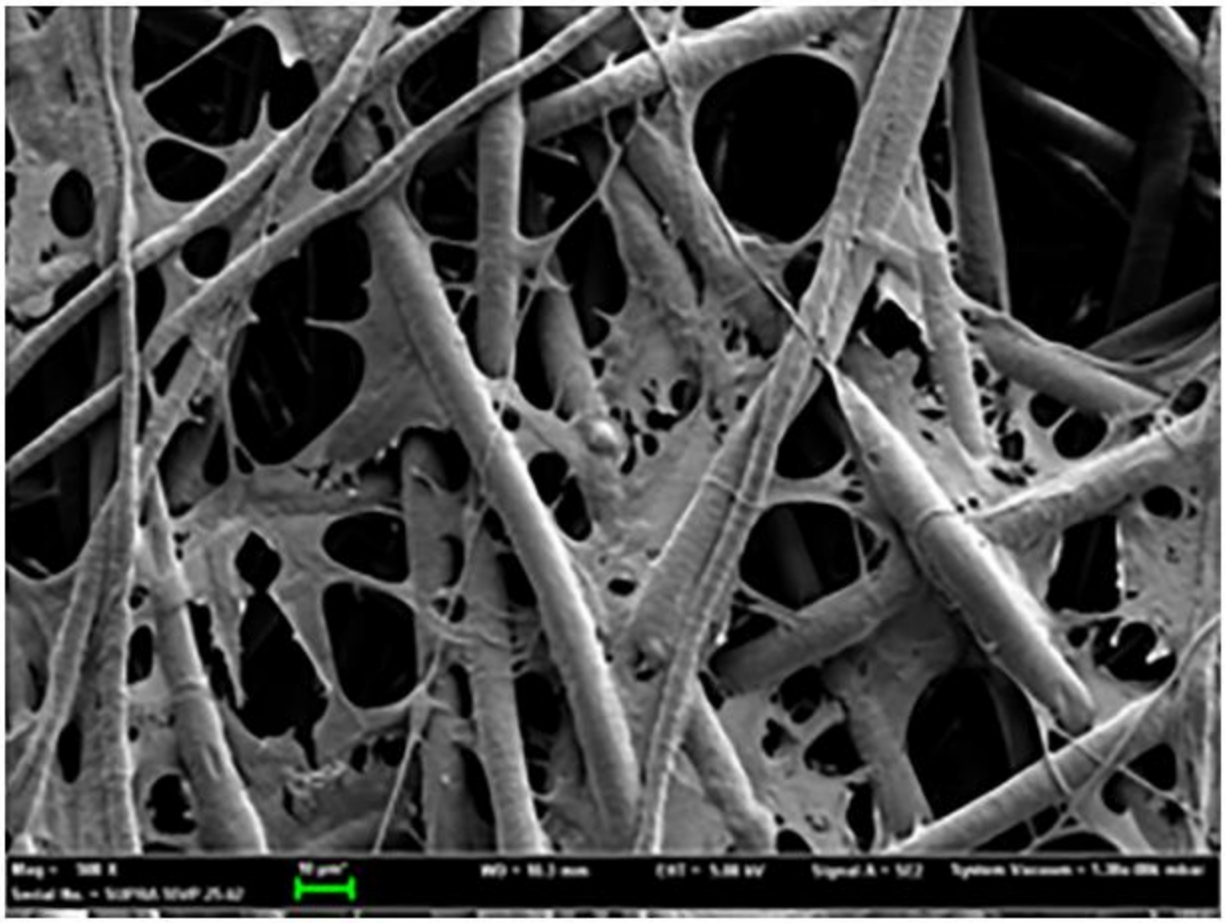

***Figure 5. PCL scaffold seeded with stem cells and neural derived stem cells*[79].**

In another study, Zhang *et al.* [79] designed a hybrid polycaprolactone/polysialic acid (PSA) electrospun scaffold loaded with methylprednisolone (MP). Before mixing the polymers together, researchers decreased PSA hydrophilicity to make it more compatible with PCL. Also, it was noted that the addition of PSA decreased the fiber diameter and pore size, **Figure 6**. The drug efficiently decreased the expression of TNF-α, IL-6 and caspase-3, pro-inflammatory mediators in SCI, and enhanced myelin formation *in-vivo* model[80].

`

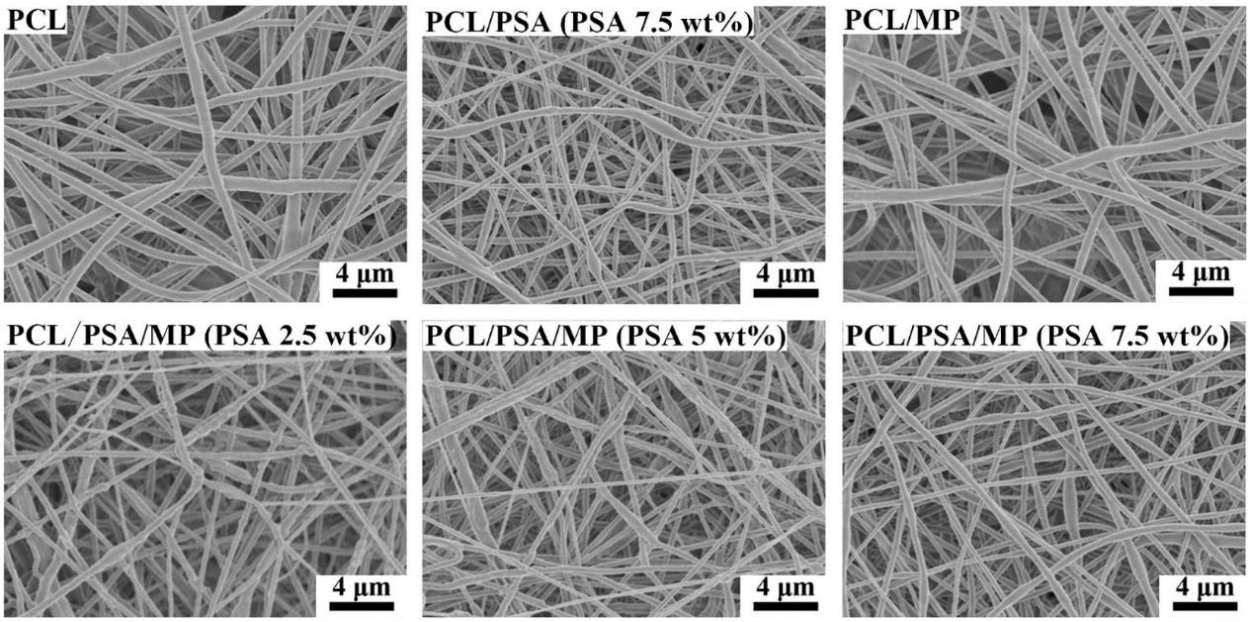

***Figure 6. Morphologies of fabricated NFs of PCL, PSA, and the drug MP, with different concentrations*[80].**

Furthermore, Neal *et al*.[80] designed a cylindrical PCL film filled with aligned PCL/laminin NFs blends and investigated the *in-vivo* activity for tibial nerve regeneration. Filled scaffold resulted in electrical conduction restoration in anterograde and retrograde direction with significantly enhanced motor function[81]. In one study, Prabhakaran et al.[81] compared the biological activity of plasma treated PCL NFs versus PCL/collagen NFs. Interestingly, the study showed that Schwann cells, peripheral myelinating cells, exhibited better morphology, attachment, and proliferation on the plasma treated PCL scaffold [82]. In addition, Nguyen *et al.*[71] designed aligned PCL-co-ethyl ethylene phosphate copolymer, mixed with micelles loaded with microRNA within a collagen hydrogel. Enhanced myelination was confirmed with Myelin-Associated Glycoprotein (MAG+) glycoprotein and aligned neurofilaments on axons and on NFs, **Figure 7**[72].

`

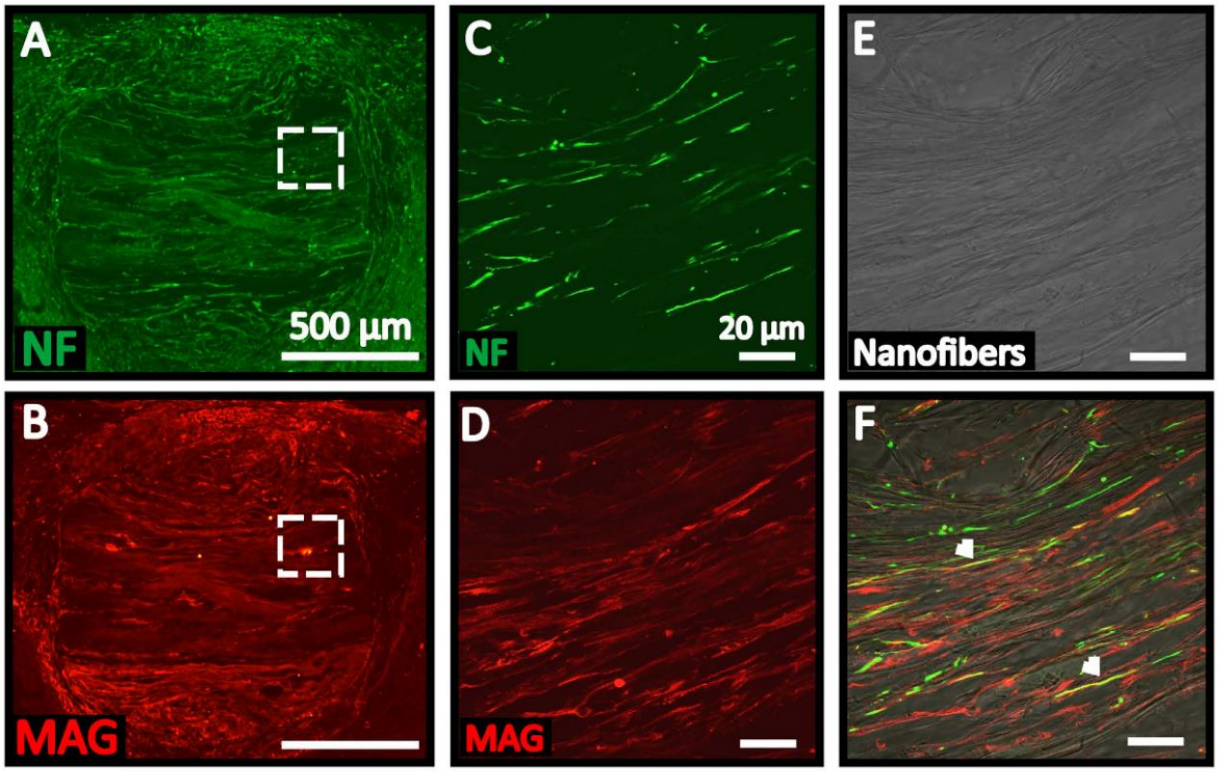

Figure 7. Regeneration of neurofilaments (NF+, green) and remyelination (MAG+, red), after 4 weeks of in-vivo implantation. (A,B) Overview of the spinal injury. (C,D) High magnification images of the insets in (A and B), respectively. (E) Bright-field image of nanofibers in (C and D). (F) Merged images of (C,D, and E)[72].

Moreover, Song *et al*.[82] fabricated PCL NFs scaffold filled with graphene oxide. Graphene oxide enhanced the thermal and mechanical properties of the scaffold. In addition, the composite scaffold increased the differentiation capacity of the low-differentiated rat pheochromocytoma (PC12-L) cells into neuro-like cells for potential use in nerve regeneration[83].

Table 1 summarizes some of the previous attempts and different designs of PCL electrospun NFs that has been fabricated and examined for neuronal regeneration after spinal cord injury (SCI) or for peripheral nerve injury (PNI) or for general neuronal tissue regeneration. So far, all the previously designed PCL NFs scaffolds were modified with single copolymer, or without modifications, except for one study where PCL/chitosan NFs where conjugated with

`

laminin. However, the study lacks in-depth analysis to the biological activity of the scaffold, and only the proliferation rate of Schwann cells was reported[84]. Thus, the investigation of the effect of dual protein conjugation on the PCL biological activity for neuronal regeneration applications is the focus of the present thesis.

Table 1. Previously prepared Polycaprolactone nanofibrous scaffolds for spinal cord or neuronal regeneration.

Ref	Design	Drug /cellular loading	Application	Comments
85	Core/Shell aligned microfibers with adequate surface roughness. Core: PCL/PANI (130:3) Shell: PLGA or PLGA/PANI (15:1)	Blank	SCI. In-vitro: A-172 cells In-vivo: male Wistar rats	Researchers used PCL to adjust degradation, yet they did not perform degradation test. Also, amount of PANI used is very small, and during conductivity tests, they hydrated the samples, which affected the results. The discussion is contradictive, as the rat group treated with the non-conductive PLGA scaffolds showed better locomotor activity in-vivo, but the paper recommends conductive scaffold.
86	Random PCL NFs seeded with stem cells and neural derived stem cells	ASCs and iPSC-NSCs	SCI. In-vivo: Wistar rats	The combination of two types of stem cells increased the expression of GDNF and NGF, but not NT3, with highest locomotor recovery score.
80	Random PCL/PSA hybrid scaffold (7.5% PSA)	Methyl-prednisolone	SCI. In-vitro: astrocytes and SH-SY5Y cells In-vivo: female Sprague Dawley rats	~80% of the drug was released in 4 h. The drug efficiently decreased the expression of TNF-α, IL-6 and Caspase-3, and enhanced myelin formation in-vivo.
72	Aligned PCL-co-ethyl ethylene phosphate copolymer, mixed with micelles loaded with drugs within a collagen hydrogel.	NT-3 or miR-222 microRNA	SCI. In-vivo: adult female Sprague Dawley rats	NT-3 had low loading capacity because it was not incorporated in micelles. 87% of proteins showed burst release in the first 24 hours. Enhanced myelination was confirmed with MAG+ glycoprotein on axons and on NFs.

`

[87]	Random PCL/collagen (3:1)	Blank	PNI. In-vitro: pool of cells	Co-cultures of cells: dorsal root ganglia explant, schwann cells, olfactory ensheathing cells and fibroblasts. Collagen directed the neurite outgrowth, however, blank PCL showed longer neurites. Also, schwann cells migrated furthest on collagen/PCL scaffold.
[88]	Aligned PCL/gelatin (7:3)	Blank	General nerve regeneration. In-vitro: stem cells (C17.2)	Fibers were better aligned with lower gelatin concentration. Fiber and pore diameter as well as contact angle and mechanical strength decreased with increasing gelatin. Neonatal mouse cerebellum (C17.2) cells showed better neuronal outgrowth and directionality.
[89]	Aligned PCL/collagen (3:1)	Blank	Axonal regeneration. In-vitro: U373 astrocytoma, hNP-Acs, and SH-SY5Y	Addition of collagen increased the fiber diameter. Astrocytoma cells adhered less on collagen/PCL than PCL and the opposite for hNP-Acs. As for SH-SY5Y, the attachment was not successful due to poor adhesion. Again, this study shows how different type of neurons interact differently on heterogenous scaffolds.
[90]	Aligned PCL/PLGA (45:55)	Blank	General nerve regeneration. In-vitro: Rat Schwann cells (CRL-2765)	The aligned NFs showed increased contact angel and decreased pore size and young's modulus than the random NFs. Actin and focal adhesion molecule (Vinculin) were detected in alignment with fiber orientation.

2.3. Hypothesis and Specific Aims

The aim of this work was to fabricate electrospun nanofibrous scaffold to promote neuronal adhesion, neurites sprouting, and axonal elongation in cases of spinal cord injuries. The backbone of the scaffold is PCL NFs, chemically conjugated post-spinning with different extracellular matrix proteins; namely fibronectin (FBN), laminin (LAM), and the peptide RGD to provide natural binding sites favorable to the neuronal cells. This post-spinning anchoring method was performed instead of co-spinning both synthetic polymer and natural protein together to by-pass exposing natural proteins to high voltage and heat through the electrospinning process. This approach is employed to maintain the maximum biological activity of the proteins by preserving their quaternary structure, which results in equal or even more promising results to conventional co-spinning method, with much lower quantities of the protein, making it more cost-effective[91].

FBN is one of the glycoproteins of the extracellular matrix. It binds primarily to membrane-bound integrin receptors[92]. LAM is another glycoprotein of the ECM that is important component of the basal lamina and plays a unique role in cell adhesion[93]. Moreover, RGD is a small tripeptide of Arginine-Glycine-Aspartate that is found to be part of the amino acid sequence of FBN, LAM, and other ECM proteins. RGD is recognized by the integrin receptors and influence cell-cell interaction[94]. Based on this background, it was hypothesized that PCL-conjugated to essential ECM proteins FBN and LAM, alone or in combination, supports neuronal cell adhesion, survival and growth. To test this hypothesis, the main primary objectives were to investigate the success of the post-spinning covalent bonding of different proteins to PCL and to test the synergistic effect of FBN and LAM employed together within the PCL NFs scaffold for neuronal adhesion and

`

sprouting as a first step in the healing process, compared to single protein immobilized PCL scaffolds.

`

3. Materials and Methods

3.1. Materials

Poly(Ɛ-caprolactone) (PCL, average molecular weight 80 kDa, Sigma Aldrich), glacial acetic acid (98%, molecular weight=60.05 g/mol, Sigma Aldrich), formic acid (99%, molecular weight = 78.13, Sigma Aldrich), citric acid (Serva, Germany), morpholinoethane sulfonic acid (MES buffer, Serva), fibronectin (FBN, Sigma Aldrich), laminin (LAM, Sigma Aldrich), RGD (Sigma Aldrich), 1-Ethyl-3-(3-dimethylaminopropyl)carbodiimide (EDC, Sigma Aldrich), N-hydroxysuccinimide (NHS, Sigma Aldrich), roswell park memorial institute culture medium (RPMI 1640, Lomza, Belgium), fetal bovine serum (FBS, Life Science Production, U.K.), penicillin-streptomycin (pen-strep, Lonza, Germany), phosphate buffer saline (PBS, Lonza, U.S.A.), 3-(4,5-dimethylthiazol-2-yl)-2,5-diphenyltetrazolium bromide (MTT reagent, Serva, Germany), glutaraldehyde (Sigma Aldrich), ethanol anhydrous (≥99.5%, molecular weight=46.07 g/mol, Sigma Aldrich), dimethyl sulfoxide (DMSO, ≥99.9, molecular weight=78.13 g/mol, Serva), Hexamethyldisilazane (Sigma Aldrich, Germany).

3.2. Fabrication of Electrospun NFs Scaffold

3.2.1. Preparation of Electrospinning Solution

PCL was dissolved in a mixture of acetic acid and formic acid (3:7) to a final concentration of 12% or 15% w/v, where 1.2 g or 1.5 g of PCL were added to 10 ml of solvent mixture in a sealed container in addition to 0.7 g citric acid (CA) (7% w/v) and left on magnetic stirrer for 3 hours at room temperature until complete dissolution[75].

`

3.2.2. Electrospinning Setup

Freshly prepared solutions were electrospun using SNAN electrospinning setup (MECC co., Ltd, Japan, **Figure 8**). Six ml syringe was filled with the electrospinning solution and connected through Teflon tubing to the needle tip placed on a stationary electrospinning stage, keeping the tip to collector distance at 15 cm. NFs were collected on an aluminum foil using a 22-gauge needle. The electrospinning parameters chosen were 20 KV, 1.5 ml/h, humidity 35-50%. After collection, NFs were left in distilled water overnight to wash remaining solvent until pH was neutral. Then NFs were cut into 1x1 cm^2 pieces and finally sterilized using UV lamp for 2 hours each side[56].

Figure 8. SNAN electrospinning setup (MECC co., Ltd, Japan)[95]**.**

`

3.2.3. Functionalization of Proteins to Electrospun PCL-NFs

After collecting electrospun 12% PCL-NFs, FBN, LAM, or RGD peptide were chemically conjugated to blank-PCL sheets via carbodiimide coupling to fabricate FBN-PCL-NFs, LAM-PCL-NFs, FBN-LAM-PCL-NFs, and RGD-PCL-NFs. First, the conjugation solution was prepared by adding a pre-calculated amount of each protein to 0.1M MES (pH 5.5) containing 0.2M EDC and 0.5M NHS. The conjugation solution was left for magnetic stirring for 30 min to allow for the activation of the amino group in the protein. Then, the final solution was pipetted over the surface of the blank-PCL meshes at a concentration of 2 µg of protein per cm^2 of surface area. The solution was maintained on the surface of the PCL-NFs for 7 h at room temperature. Afterwards, the fibers were washed in PBS[91].

3.3. Characterization

3.3.1. Morphological and Structural Characterization

The morphology of the electrospun 12% and 15% PCL-NFs was observed using Field Emission Scanning Electron Microscopy (FESEM, Leo Supra 55, Zeiss Inc., Oberkochen, Germany) to determine the optimum PCL concentration and electrospinning parameters to obtain smooth droplet-less NFs. Prior to imaging, previously prepared samples were gold sputtered at 15 mA for one min to increase conductivity (LADD Hummer 8 Sputter Coater). The diameter of NFs was measured using ImageJ® software, where two sets of measurements were calculated for each scaffold at random positions. Each set included at least 40 NFs. Statistical analysis for mean and standard error calculation of size distribution and average fiber diameter sizes was performed using GraphPad Prism 7 software[56]. The surface area of the 12% and 15% PCL-NFs was compared. For this, the Brunauer–Emmett–Teller (BET) surface area was calculated through the nitrogen gas

`

physical adsorption method with a surface area analyzer (NOVA touch 2LX, Quantachrome Corporation, USA) at 77°K. Before BET measurement, degassing of all samples was performed in a vacuum oven at room temperature for 24 h. The relative pressure range P/P0 selected was 0 to 1 for calculating the BET surface area with a Nova Enhanced Data Reduction Software[55]. To determine the porosity of both concentrations of PCL-NFs fabricated, the thickness of the scaffolds was measured using a micrometer (Mitutoyo, Japan). Then, their apparent density and porosity were estimated through direct substitution in Eqs. (1) and (2) respectively[96].

$$Apparent\ density\ (g\ cm^{-1}) = \frac{Mass\ of\ scaffold\ (g)}{Scaffold\ thickness\ (cm) \times Scaffold\ area\ (cm^2)} \quad (1)$$

$$Prosity\ (\%) = \left(1 - \frac{Scaffold\ apparent\ density\ (g\ cm^{-3})}{bulk\ density\ of\ PCL\ (g\ cm^{-3})}\right) \times 100\% \quad (2)$$

Energy-Dispersive X-ray spectroscopy equipped within the FESEM (EDX, Zeiss Inc., Oberkochen, Germany) was used to detect the presence of nitrogen in the RGD-PCL-NFs, compared to the blank-PCL-NFs[56]. To analyze the chemical conjugation of FBN, LAM, and RGD to the PCL-NFs mats, Attenuated Total Reflectance - Fourier transform infrared spectroscopy (ATR-FTIR, Thermo-scientific, Nicolet 380, USA) measurements were carried out[56]. Transmission peaks were measured in the range of 400–4200 cm^{-1}.

3.3.2. *In-vitro* Stability Tests

For swelling measurements, dry samples of PCL-NFs and protein conjugated PCL-NFs were soaked in artificial cerebrospinal fluid (aCSF, pH=7.3). aCSF is composed of 10 mM glucose, 3.2 mM potassium chloride, 120 mM Sodium chloride, 1 mM sodium phosphate monobasic anhydrous, and 26 mM sodium bicarbonate[97]. Different samples were weighed (W_1) then soaked in aCSF at 37°C. Soaked samples were removed after 48 h, and excess aCSF on the surface of the

`

samples was removed using filter paper, then samples were weighed again (W_2). At least three samples of each type of fibers were used. The degree of swelling (Sw%) was estimated through direct substitution in Eq. (3).

$$Sw\ (\%) = \left(\frac{w_2 - w_1}{w_1}\right) \times 100 \quad (3)$$

where W_1 is the weight of dried samples before soaking and W_2 is the weight of soaked samples.

For the degradation measurements, different samples of PCL-NFs and protein conjugated PCL-NFs were again weighed (W_i) and soaked in aCSF, pH=7.3, at 37°C for three months in water bath. Soaked samples were removed at time interval each month, air dried for one hour, then samples were weighed (W_x), then soaked again in aCSF. At least three samples of each type of fibers were used. The degree of weight change was estimated at each time interval through direct substitution in Eq. (4).

$$W\ (\%) = \left(\frac{w_x - w_i}{w_i}\right) \times 100 \quad (4)$$

where W_i is the weight of samples before soaking and W_x is the weight of dried samples after soaking. At the end of the degradation test, ATR-FTIR measurement was done to examine the changes in the chemical structure of different scaffolds.

3.4. Biological Assessment

3.4.1. *In-vitro* Cell Culture

Neuroblastoma SH-SY5Y cell line was used. Cells were cultured as monolayer in Roswell Park Memorial Institute Medium (RPMI 1640) supplemented with 10% FBS and 1% penicillin/streptomycin mixture, in a humified incubator supplemented with 5% CO_2 at 37°C.

`

Media was replaced every three days. When cells reached 70% confluency, they were detached and passaged at 1:3 ratio. The third to fifth passages of SH-SY5Ys were further used for seeding UV-sterilized scaffolds. Different scaffold samples were cut into 0.5 x 0.5 cm^2 and placed in triplicates in a 24-well plate. Each well was seeded with 10,000 cells per well and plates were incubated in a humidified atmosphere at 37 °C and 5% CO_2 for further cell viability and adhesion tests.

3.4.2. Cells Viability and Proliferation

To determine the biocompatibility of different PCL scaffolds, cellular viability and metabolic activity was determined by the calorimetric MTT assay as described previously[98], at day two and five of the cultivation. Wells were incubated with 100 µl of 12 mM MTT reagent, at 37°C for 4 h, followed by solubilization of the formed formazan dye using DMSO. The produced violet color was measured using microplate spectrophotometer (SPECTROstar Nano, BMG LABTECH, Germany) at 540 nm.

3.4.3. Quantification of Neurite Outgrowth

At day five of the experiment, the length of the extended neurites (N = 40) from the cells were measured from the cell body to the tip of the process using ImageJ® software. Statistical comparison was calculated using one-way ANOVA with Dunnett's test for multiple comparisons (GraphPad Prism).

3.4.4. Cells Adhesion and Spreading

To investigate attachment of SH-SY5Y cells on the fabricated PCL scaffolds, light microscopy as well as FESEM images were taken. Light microscopy (Zeiss, Olympus DP-100

`

camera) was used for follow-up morphology and status of the living neuroblastoma throughout the experiment. Image filters were used to increase the contrast of light micrographs. At the end of the experiment, each nanofibrous scaffold was immersed in one ml of McDowell and Trump's Fixative solution for 30 min to fix cells on the scaffold. Hexamethyldisilazane, 0.5 ml, was then added for 10 min. Finally, NFs scaffold were left to air-dry overnight. Dry constructs were sputter coated with gold for 1 min and observed by FESEM as described previously.

To assess cellular morphology, the projected area (A) and perimeter of cells (P) (N = 30) were analyzed by the ImageJ® software. The shape index was estimated through direct substitution in Eq. (5)[99]. Statistical comparisons for shape index and projected area of cells were measured using one-way ANOVA with Dunnett's test for multiple comparisons (GraphPad Prism).

$$Shape\ Index = \frac{4\pi A}{P^2} \quad (5)$$

3.5. Statistical Analysis

Each experiment was performed in at least triplicates. All means and standard error were calculated using the software GraphPad Prism 7.0. Results are presented as mean ± SEM, and statistical significance was confirmed using a one-way ANOVA, with p-values equal *$p < 0.05$, **$p < 0.01$, ***$p < 0.001$, and ****$p < 0.0001$.

`

4. Results and Discussion

4.1. Fabrication and Morphological Analysis

The solvent used in the preparation of the spinning solution is a combination of two benign solvents (formic acid and acetic acid), to avoid any possible toxicity from the remaining traces of the solvent in the fabricated PCL-NFs. These solvents support green synthesis and did not affect the quality of the produced NFs[100]. At the beginning, I prepared a solution of 8% PCL, the low concentration did not spin, so I increased the spinning solution concentration to 12% and 15%. FESEM images were taken to assess the electrospinning parameters of PCL-NFs with different polymer concentrations: 12% and 15%. To obtain smooth fibers, different parameters were optimized, including the gauge diameter of the nozzle, flow rate, and applied voltage. The nozzle gauges used were 27, 22, and 18. At each voltage, the flow rate was modified until a jet fibers shower was produced. This step was repeated over a range of voltages and flow rates, using the normal clip spinneret setup, **Figure 9**. The optimization was repeated for both 12% and 15% PCL solutions. The collection was performed on an aluminum foil station. To allow easy removal of NFs mats, a piece of clean gauze was placed on the aluminum. However, the NFs collected on gauze had rough surface compared to NFs spun directly on aluminum foil, thus, I decided to continue electrospinning without gauze. Moreover, a core-shell spinning trial was examined using the coaxial spinneret setup, **Figure 9**. A 10% polyvinyl alcohol (PVA) was prepared as the shell, and PCL solution was filling the core syringe. Unfortunately, upon co-spinning, when the PVA solution meets the PCL solution at the tip of the nozzle, the PCL coagulate and block the nozzle. This is due to the hydrophobic nature of PCL.

`

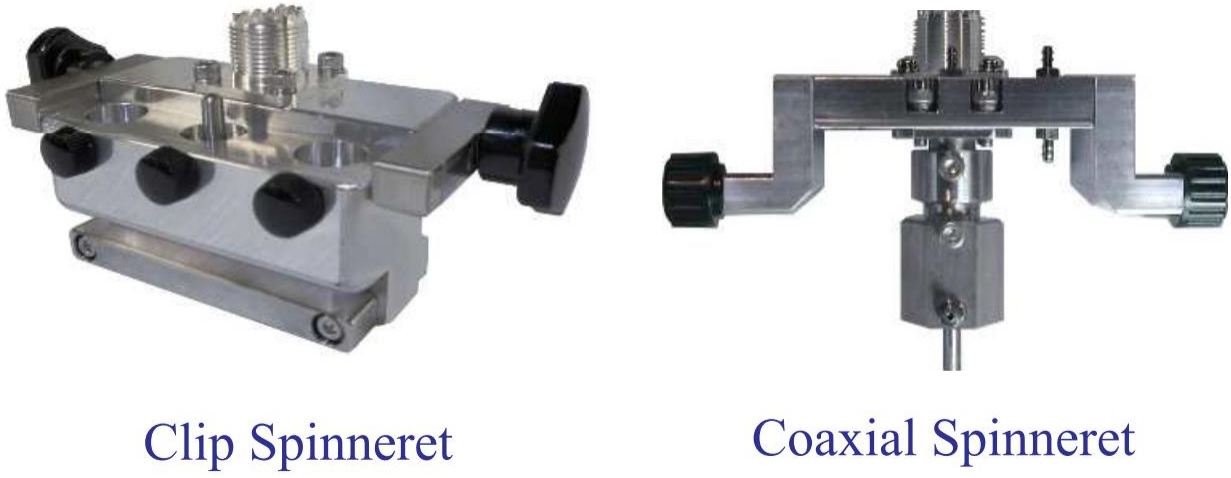

Figure 9. Different spinnerets setup, SNAN (MECC co., Ltd, Japan)[95] **.**

The optimal electrospinning parameters were determined to be 20 KV, 1.5 ml/h, at a working distance of 15 cm. The micrographs in **Figure 10** show randomly interconnected smooth, non-beaded NFs for both formulations, similar to the natural ECM. The average fiber diameter distribution was in the range of 200 – 600 nm for the 12% PCL-NFs, with a mean diameter of 358.8 ± 9.2 nm. On the other hand, the 15% PCL-NFs resulted in significantly higher fiber diameter distribution in the range of 600 – 1100 nm with a mean diameter of 887.2 ± 11.6 nm. This higher fiber diameter distribution at the higher concentration has been previously reported in the literature[75]. After the optimization of the spinning solution and parameters, I started preparing larger volume of spinning solution ready for collection, to decrease the variability that might rise from a preparation to another. The spinning of large volumes might take two or three days. On the second day, the solution consistency varies, and the spinning is not homogenous. It was observed that the viscosity appeared to be less on the following days. This is probably due to the effect of water vapor in the atmosphere that acts in the degradation of formic acid and the hydrolysis of the

`

polyester backbone is enhanced in these conditions[100]. Therefore, the solution must be freshly prepared before electrospinning.

The porosity of PCL-NFs mats was calculated using the reported density of PCL (1.145 g/cm^3) and the calculated apparent density of the electrospun PCL[96]. Moreover, the specific surface areas of the PCL-NFs were calculated using the nitrogen absorption/desorption isotherms[55]. These results are summarized in **Table 2**.

Table 2. Diameter, apparent density, porosity, and surface area of the PCL-NFs scaffolds.

PCL-NFs Formulation	**Diameter (nm)**	**Apparent Density (g/cm^3)**	**Porosity %**	**Surface Area (m^2/g)**
12%	358.8 ± 9.2	0.19 ± 0.04	82.86 ± 3	652 ± 16
15%	887.2 ± 11.6	0.19 ± 0.05	83.38 ± 4	254.2 ± 39

Porosity is one of the crucial parameters in tissue regeneration applications to allow the infiltration through the scaffold. It should also ensure nutrient and metabolite exchange across its structure. To fulfill these requirements, desired porosity value reported should generally be greater than 60%[96]. Our results indicate that the pores within the manufactured PCL-NFs (>80%) are favorable for nutrient exchange and would support vascular permeability through the porous structure of the scaffold. Furthermore, the high specific surface area characterizing the fabricated NFs is highly favorable for the chemical functionalization during the fabrication process[101]. The high surface area of the nanofibrous scaffolds would likely provide a suitable platform for the interaction with the cells by allowing attachment, elongation and development of connections between cells[75]. From the current results, the 12% PCL formulation was chosen for further investigations, as it showed significantly lower fiber diameter distribution and higher surface area.

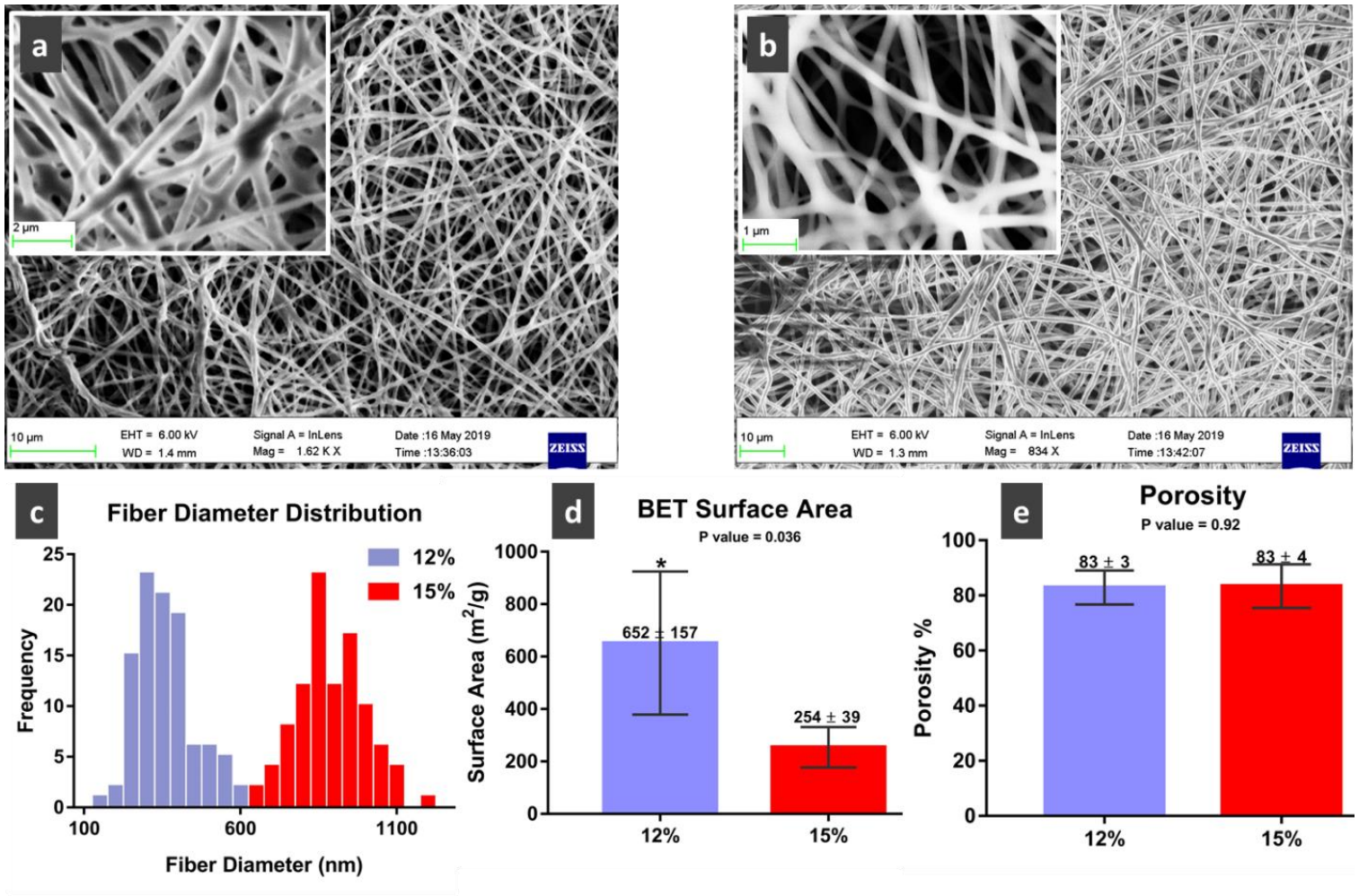

Figure 10. FESEM images of PCL-NFs: (a,b) 12% and 15% PCL formulations, (c,d,e) fiber diameter distribution, surface area analysis, and porosity, respectively. One-way ANOVA; *p < 0.05.

4.2. Chemical Analysis of Protein-Conjugated-PCL-NFs

The carbodiimide conjugation after spinning is a reliable processing technique to attach the desired proteins to the scaffold[91]. This post-spinning anchoring method was performed instead of co-spinning both synthetic polymer and natural protein together to by-pass exposing natural proteins to high voltage and heat through the electrospinning process. This approach is employed to maintain the maximum biological activity of the proteins by preserving their quaternary structure, which results in equal or even more promising results to conventional co-spinning method, with much lower quantities of the protein, making it more cost-effective[91].

The mechanism of carbodiimide conjugation is represented in **Figure 11**. Briefly, in aqueous medium, EDC is protonated to an active carbocation attacking ionized carboxylic groups and forming O-acylisourea intermediate, which is unstable. Following this, the activated O-acylisourea form an amide bond with the amino groups present, along with a urea byproduct. The addition of NHS forms a more stable intermediate to allow for more efficient conjugation reaction[102]. The first conjugation attempt of PCL to proteins was conducted in water. After few hours, white precipitation could be detected in the beaker which could be EDC or protein degradation. To solve, this, I controlled the pH value of the reaction medium using MES buffer at 5. The addition of buffer resulted in clear and stable reaction. It is previously reported in literature that the amide bond forms easily at pH 5-7[102].

`

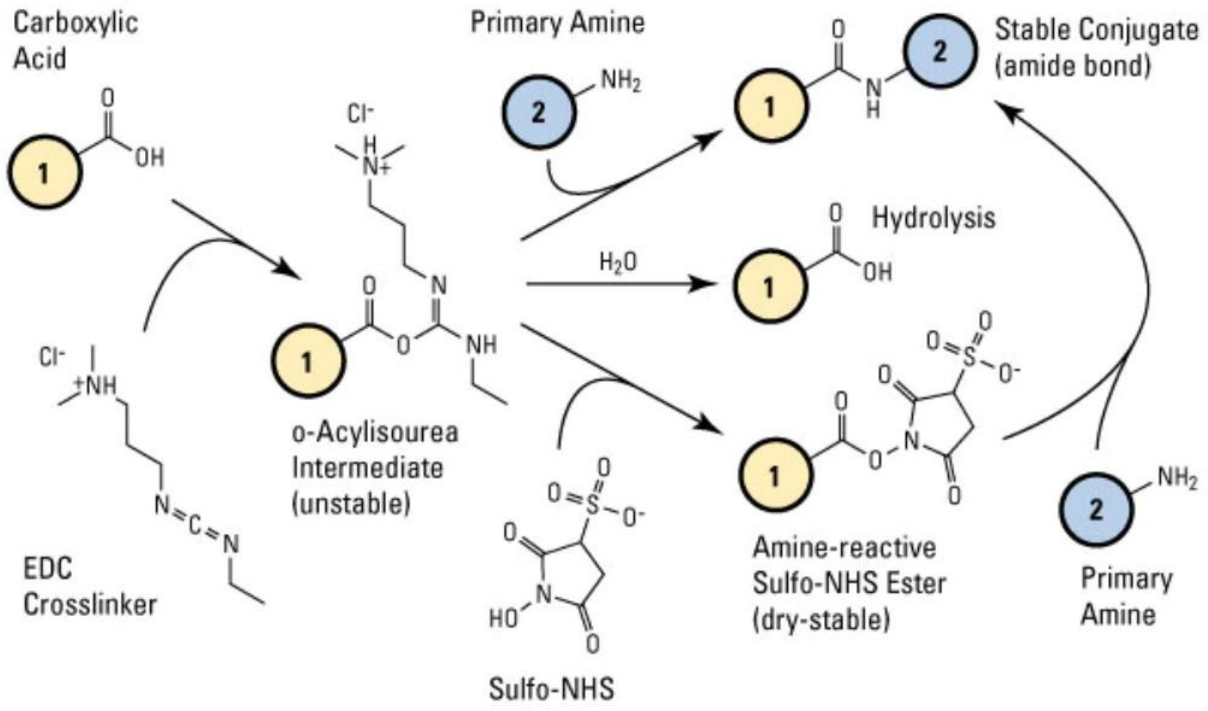

Figure 11. Carbodiimide conjugation mechanism and amide bond formation[103]**.**

To evaluate the conjugation of proteins to the PCL-NFs mats, a pilot experiment using RGD peptide was performed first. The EDX analyzer is an added detector to the FESEM setup. It detects the specific X-ray emitted during relaxation of excited electrons after hitting atoms with high energy beam of electrons[104]. The EDX analysis confirmed the presence of nitrogen pertaining to the peptide in the RGD-PCL-NFs and its absence in the blank-PCL-NFs, **Figure 12a**. Additionally, the morphology did not change after the post-spinning chemical conjugation of RGD to the PCL-NFs, **Figure 12b**. ATR-FTIR analysis was conducted to closely examine the post-spinning EDC-NHS treatment and the presence of the different proteins (FBN, LAM, and RGD) on the PCL scaffolds. **Figure 12c shows** the transmittance spectra of all protein-conjugated-PCL-NFs, and the spectrum of blank-PCL (Spectrum 1), was included as control for comparison. Blank-PCL showed characteristic absorption bands at 2939 and 2867 cm^{-1} associated with alkyl C-H

`

bond stretch. Also, intense C=O and C-O stretching peaks can be detected at 1724 and 1043 cm^{-1}, respectively[105]. It is noted that the main peaks of blank-PCL structure are present in all other spectra. However, the intensity of the C=O peak decreased due to the conjugation of peptides[105]. Further, a stretching peak corresponding to O=C=O appears between 2351 and 2358 cm^{-1}, with varying intensities, which could be attributed to adsorbed CO_2 gas in the samples from ambient environment[106]. After addition of the RGD to PCL (Spectrum 2), different peaks appeared at 3670, 1649 and 1402 cm^{-1}, attributed to O-H bond stretch, C=O stretch of amide I and N-H of amide III of RGD peptide, respectively[105]. Moreover, FBN- and LAM-conjugated PCL-NFs (Spectra 3, 4, and 5) showed extra characteristic peaks. Thus, the N-H stretching vibrations of amide A and B of both FBN and LAM are extended as a slightly board peak at ~3400 cm^{-1} [107]. It can also be observed that the vibrational frequency of the amide I of the globular proteins FBN and LAM is located at 1593 – 1596 cm^{-1}, which is almost below the lower limit of the frequency range for amide I (normally 1600 – 1700 cm^{-1}) [108]. Amide I vibration is highly affected by the protein backbone not side chains; thus, it is sensitive to the secondary structure of the protein, i.e alpha helix and beta sheet of the protein, which are defined by the organization of hydrogen bonding between carboxylic oxygen and the amino groups present in the backbone of the proteins. The interaction between these hydrogen bonds have been proven theoretically to lower the frequency of the amide I, as observed in our reported spectrum[107,108]. Since amide II is strongly coupled to the amide I, this would explain the lower peak frequencies attributed to the in-plane bending vibration of amide II (C-N and N-H bonds) in the FBN and LAM curves, at 1429 cm^{-1} [108].

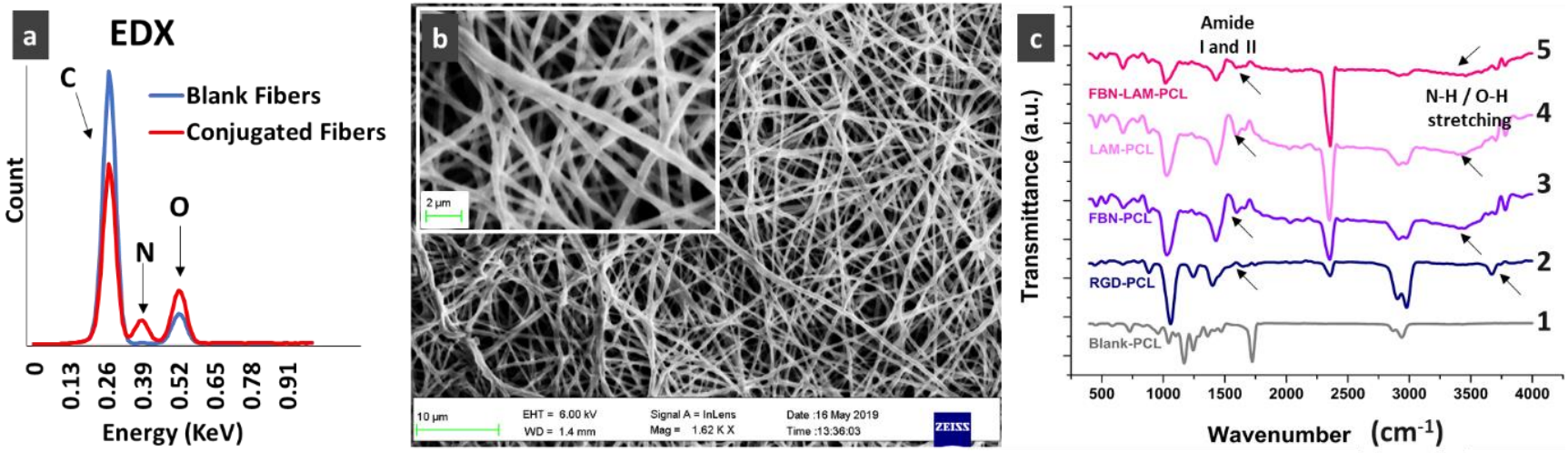

Figure 12. Post-conjugation analysis: (a) EDX spectra of blank-PCL and RGD-PCL showing the nitrogen element in the conjugated fibers and its absence in the blank fibers, (b) FESEM image of RGD-PCL-NFs, and (c) ATR-FTIR transmittance spectrum of [1] blank-PCL, [2] RGD-PCL, [3] FBN-PCL, [4] LAM-PCL, and [5] FBN-LAM-PCL NFs, with arrows pointing the amide I and II at ~1590 cm^{-1}, ~1430 cm^{-1}, and NH, OH stretch at ~3670 cm^{-1}.

4.3. *In-Vitro* Stability of PCL-NFs Scaffolds

Physical stability of the fabricated NFs was assessed by measuring the amount of water uptake after two days of incubation in artificial cerebrospinal fluid at 37°C and also the degradation rate reported as weight loss percentage over a period of three months under the same conditions. The water uptake profile of different PCL-NFs formulations is shown in **Figure 13a**. The swelling of all fibers did not differ statistically, except for the FBN-LAM-PCL-NFs, which showed significantly lower value. Mean values were 46.5 ± 4.6 %, 40 ± 3.6 %, 52.27 ± 6.4 %, 33.4 ± 2.7 %, and 12.43 ± 7.7 % for the blank-PCL, RGD-PCL, FBN-PCL, LAM-PCL, and FBN-LAM-PCL NFs, respectively. The water uptake of NFs mats was controlled by the surface area and porosity of the electrospun NFs[109]. Herein, the water uptake behavior is random without a hallmark predicted pattern. This variability has been reported previously for many synthetic and natural polymers[110]. Also, the extent of water uptake of all NFs observed in this study is low compared to other NFs scaffolds fabricated with hydrophilic natural and synthetic polymers[56,111], which is mainly due to the hydrophobic nature of PCL[109,111,112].

After three months of incubation in the artificial cerebrospinal fluid, the different PCL-NFs mats evidenced a weight loss between 10% and 20% from the original weight, **Figure 13b**, with the lowest degradation rate observed for the blank-PCL-NFs. PCL is an aliphatic polyester, which degrades primarily through hydrolytic cleavage of the ester bonds constituting the backbone chain. Thus, the long polymer chains are converted into shorter ones with smaller molecular weight, and degradation continues to yield the final product, 6-hydroxylcaproic acid, which is more water soluble[78,109], **Figure 14**. Generally, PCL is known to have a very slow degradation rate, which is desired in case of neuronal regeneration to accommodate the slow regeneration rate of neuronal

`

tissue, and limited clearance from the closed spinal cavity, thus, fast biodegradation of the inserted scaffold might accumulate by-products[69,77,109]. Also, proteins conjugated PCL-NFs showed slightly higher weight loss, which might be attributed to physical changes that occurred like increased hydrophilicity[112,113]. From the results, as-spun PCL NFs had adequate physical stability in simulated body fluid and did not require further crosslinking. This is highly favorable since crosslinking of polymers results in decreased flexibility and softness[114], confounding the fact that neurons attach better with higher survival potentials on soft substrates[115].

Furthermore, the ATR-FTIR analysis, **Figure 13c**, was conducted at the end of the experiment to elucidate the chemical structure of the scaffolds. A strong and wide absorption peak at ~3400 cm^{-1} can be noticed in curves 1 and 2 of the blank-PCL and RGD-PCL NFs, which corresponds to stretching of the newly formed OH bonds during the degradation of the backbone of the PCL[109], up until the formation of 6-hydroxylcaproic acid end-product[78]. On the other hand, the O-H absorption peak is not detected in the curves of FBN-PCL, LAM-PCL, and FBN-LAM-PCL mats (Curves 3, 4, and 5). This could be attributed to the conformational state of the conjugated FBN and LAM to PCL, which could expose more hydrophobic functional groups and mask the hydrophilic intermediate OH groups formed during degradation[92,93,116]. However, since these absorption curves did not show distinguished functional groups peaks nor amide I and II peaks, it is more likely FBN and LAM had already been released earlier.

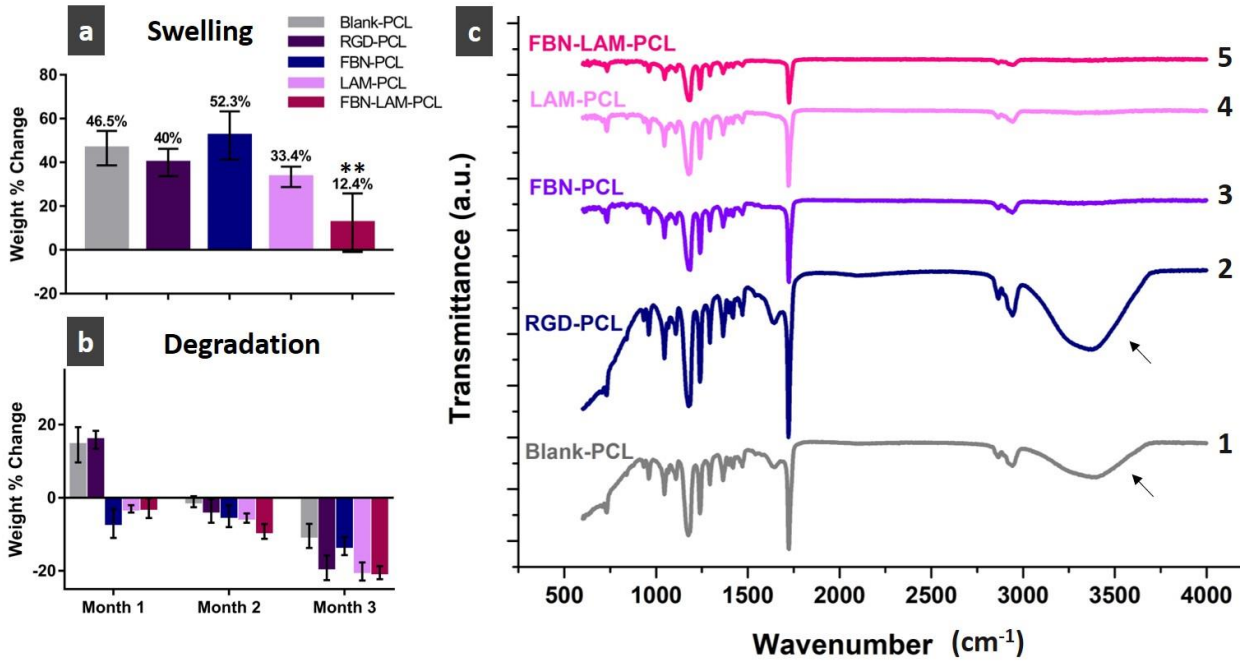

Figure 13. Stability test for fabricated PCL-NFs mats: (a) swelling percentage and water uptake after two days of incubation in aCSF; One-way ANOVA; **p < 0.01, (b) degradation rate and weight loss over three months of incubation in aCSF, and (c) ATR-FTIR transmission peaks for different PCL-NFs at the end of the experiment; [1] blank-PCL, [2] RGD-PCL, [3] FBN-PCL, [4] LAM-PCL, and [5] FBN-LAM-PCL NFs, with arrows pointing the OH stretch at 3400 cm^{-1} in curves 1 and 2 only.

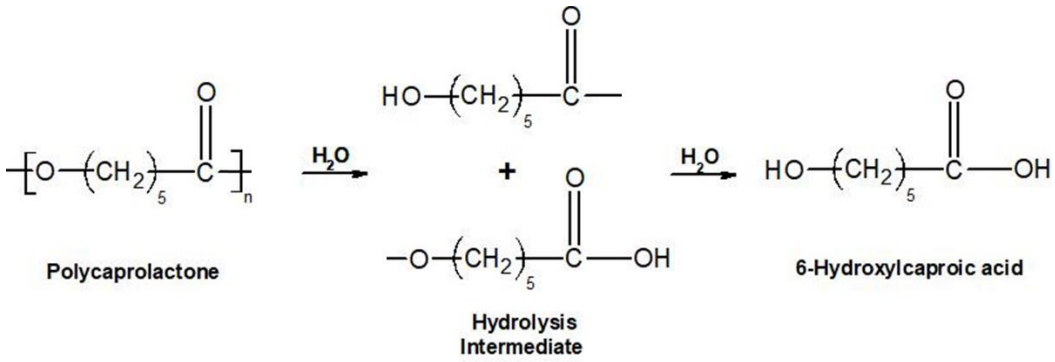

Figure 14. Schematic diagram of the hydrolytic degradation process of PCL.

`

4.4. Biocompatibility and Neurite Outgrowth Potentials of PCL-NFs Scaffolds

The neuroblastoma cell line SH-SY5Y was chosen to represent neuronal cell model as they can be differentiated into neuronal-like cells, where the rate of cells proliferation decreases, and cells extend processes reminiscent of neurite outgrowth[117,118]. The biological assessments highlight the potential of the different fabricated PCL scaffolds. The MTT calorimetric test results reported in **Figure 15** show the relative viability of neuroblastoma cells seeded on all PCL-NFs compared to control sample without fibers, at day two and five of the *in-vitro* cell culture. Initially, the seeding density was relatively low, ~10,000 cells per well for all groups, this few population can impose environmental stress and decrease proliferation rate[119]. At day two, all groups showed a steady proliferation, however the metabolic activity of cells attached to LAM- and FBN-LAM-PCL scaffolds was higher than other groups, and control cells had the lowest metabolic activity and proliferation. This could be attributed to the extra support provided by the NFs and their microfeatures, which has been shown to support cells communication, contact guidance and attachment despite the very low seeding density[120]. Also, scaffolds containing LAM led to the highest metabolic activity, because LAM is an important glycoprotein in development of the central nervous system[117]. Further, at day five of seeding, the number of cells growing on fibrous scaffolds did not increase as high as compared to the control group, indicating an induction of neuronal differentiation, where neuroblastoma cells are transformed to more neuronal-like cells under the influence of the nanofibrous scaffolds and proteins[57,117,121].

`

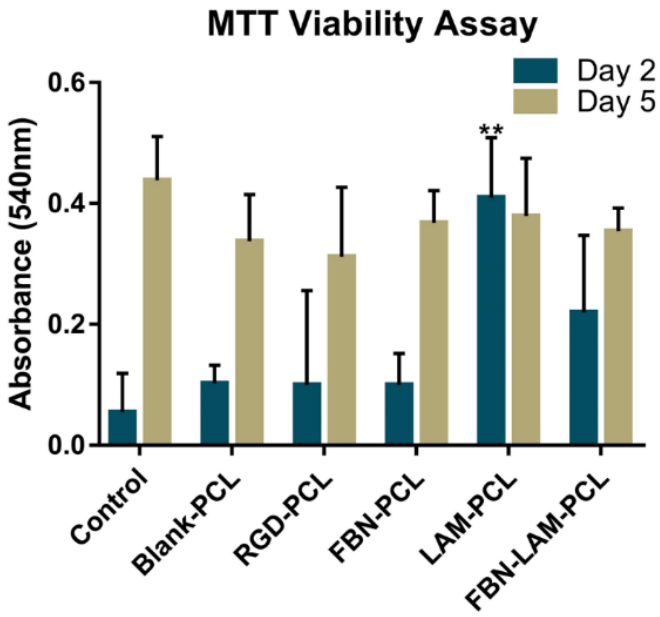

Figure 15. Viability test results using the MTT absorbance at day 2 and 5 of SH-SY5Y cell culture on different fabricated PCL-NFs; One-way ANOVA; **p < 0.01.

Cell culture images under light microscopy and FESEM were used to evaluate the neuronal morphology. Before taking SEM images, the samples should be dried. The common method is ethanol dehydration, and this is what I first used according to previously reported protocols[122]. Constituents and protocol of solutions and buffer used in the drying process are included in appendix I. However, the ethanol dehydration process did not retain the required details of morphology, it also caused structure break in cells, **Figure 16b**. Thus, I skipped the serial washing and ethanol dehydration, and used only fixation for 30 mins followed by addition of hexamethyldisilazane and let the samples to air dry, **Figure 16c**. Hexamethyldisilazane is a very volatile compound and it decreases the surface tension on the cells during the drying process and preserve so many of the details of the microstructure of cells[122,123]. Another optimization parameter for the FESEM images was to select the duration of sample exposure to gold sputtering. Higher

`

exposure time (3 mins) resulted in the deposition of more gold layers, which masked the features and details of the cellular morphology, **Figure 16a**. Thus, the selected time exposure was set to only 1 min.

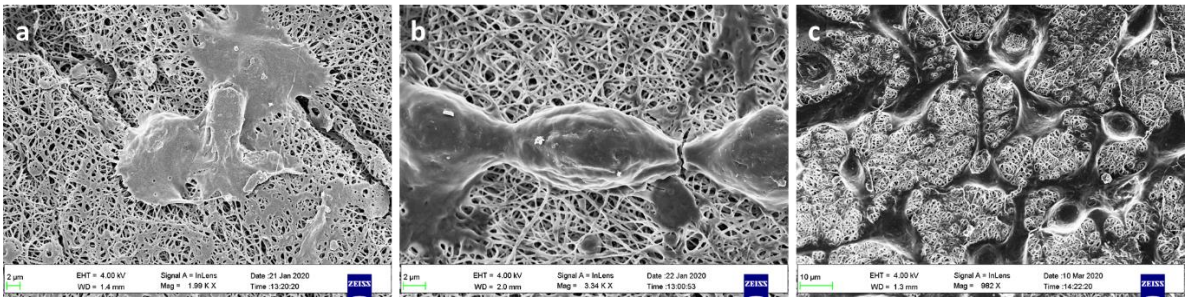

Figure 16. Results of optimization of drying process and FESEM imaging; (a) ethanol dehydration at 3 mins gold sputtering, (b) ethanol dehydration at 1 min gold sputtering, and (c) hexamethyldisilazane drying at 1 min gold sputtering.

A close look to the micrographs of *in-vitro* cell culture in **Figure 17 and 18** gives us a better understanding to the cell/scaffold interaction. After one day of the seeding, all neuroblastomas had circular non-evolved shape. Over the five-days period of the study, each group exhibited different morphology. The control cells remained mostly circular and did not project clear neurites, whereas blank-PCL scaffold stimulated the outgrowth of short neurites, although many cells showed clumped and clustered circular shape, see **Figure 17 and 18a**. Besides, all proteins-conjugated scaffolds demonstrated augmented cellular spread and polar morphology, which will be discussed in the following section. The graph in **Figure 18f** summarizes the neurite outgrowth of cells, showing all cells grown on NFs to have significantly longer processes, with the highest length for the scaffolds containing both LAM and fibronectin, with more branching and connection. Further, two-way ANOVA multiple comparison confirmed the significant enhancement in the dual protein conjugation of FBN-LAM-PCL-NFs compared to other formulations. The developing neuronal network suggests the evolution of growth cones at the tips

`

of the projected neurites, involved in pathfinding process as a response to the extracellular cues[124]. These results revealed enhanced attachment and neuronal network formation between the randomly grown cells on the dual protein-conjugated fibers. This is due to the stimulating effect of topographical cues of the NFs, combined with the extracellular proteins support[125].

The morphological analysis of the seeded cells on all PCL-NFs with shape index and the cell area of different groups calculated at day one and four of the experiment. The shape index (SI) of cells has a value between zero (linear) and one (circular), while the projected area of cells represents the likelihood of cell spreading and growth[99]. Interestingly, cells on the formulation of NFs containing both FBN and LAM together resulted in the significantly lowest SI among all groups. This result again highlights the synergistic mechanism between the dual proteins attached onto the scaffolds, strongly inducing the differentiation of neuroblastoma cells to more polar neurons[125,126]. Meanwhile, cells on FBN-PCL and LAM-PCL NFs mats have shown similarly low shape index. As for the cells grown on RGD-PCL NFs, they did not exhibit great difference in SI from day one to day four, because they already had the lowest value at day one. It is also noted that neuroblastoma cells on the blank-PCL had the higher SI, which is explained by the hydrophobic nature of PCL, which likely limited the differentiation of the cells into a more elongated morphology[112,127].

`

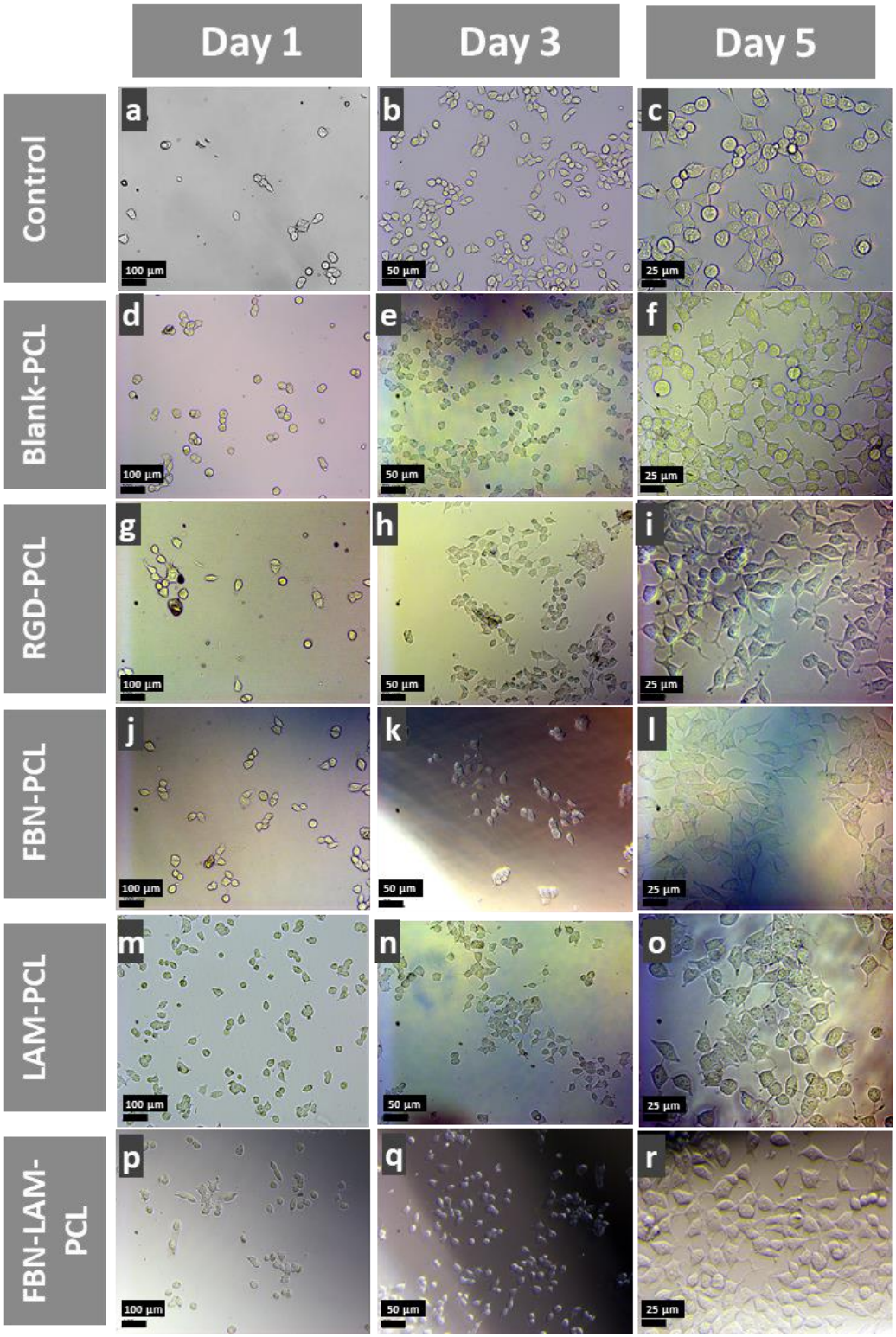

Figure 17. Light microscope graphs of in-vitro cell culture of neuroblastoma cells at day 1, 3, and day 5 of the experiment, for control, blank-PCL, RGD-PCL, FBN-PCL, LAM-PCL, and FBN-LAM-PCL groups. Image filters were used to increase the contrast of micrographs.

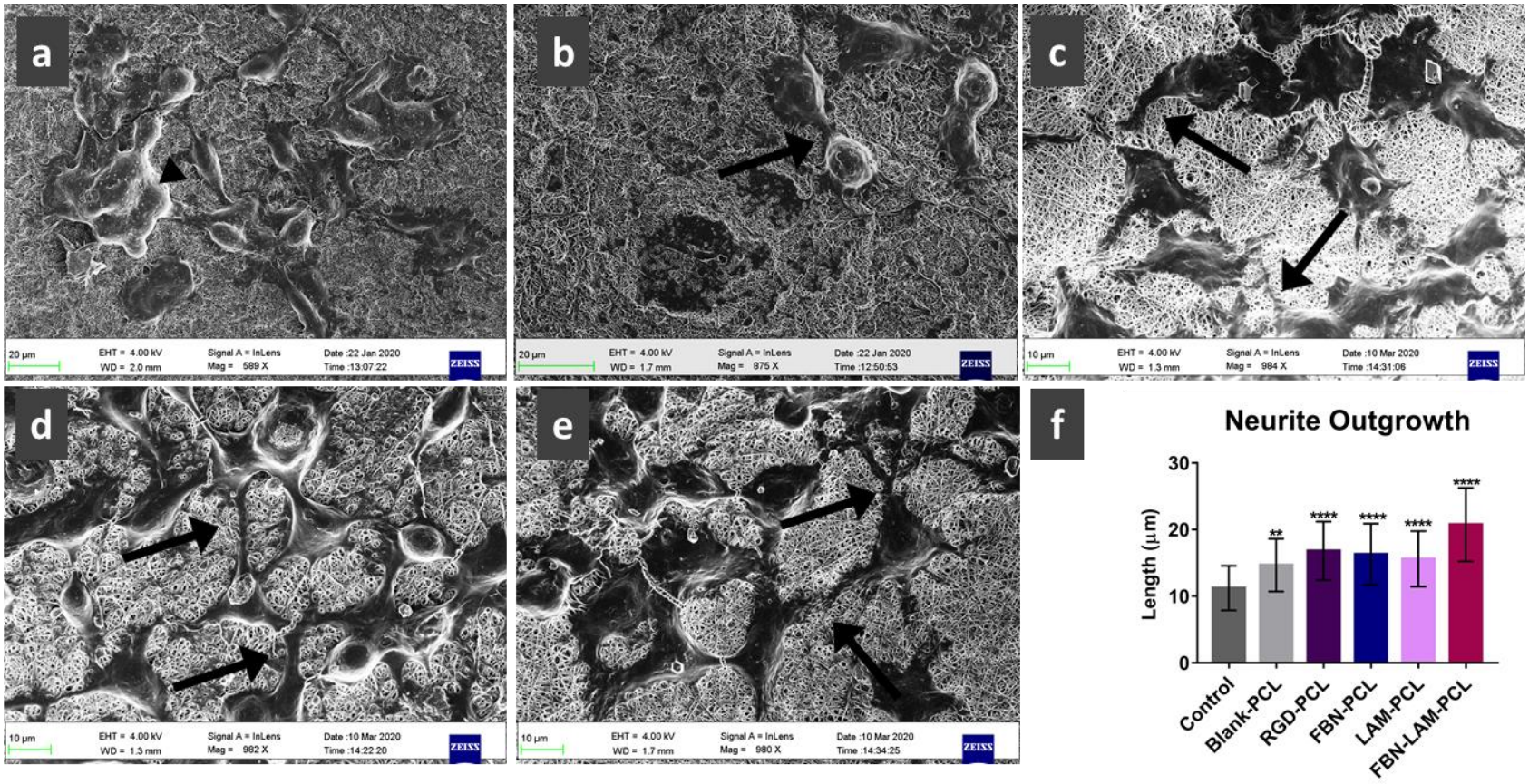

Figure 18. SEM micrographs of in-vitro cell culture of neuroblastoma cells at day 5 of the experiment, for (a) blank-PCL, black arrow head pointing clustered neuroblastomas , (b) RGD-PCL, (c) FBN-PCL, (d) LAM-PCL, (e) FBN-LAM-PCL groups, black arrows pointing the connections formed between cells, and (f) measurements of neurite length; One-way ANOVA; **p < 0.01, and ****p < 0.0001, analyzed from light microscope images at day 5 of in-vitro cell-culture.

Furthermore, the projected area of the cells on the different NFs, **Figure 19c**, is significantly higher than the control group, especially with the FBN and LAM formulations, which highlights an enhanced cellular attachment and smooth spread of cells on the fabricated PCL-NFs. Taken altogether, these results suggest that the dual combination of FBN-LAM within the PCL-NFs outranked other formulations in its bioactivity, cellular attachment, and neuronal development, simulating natural ECM.

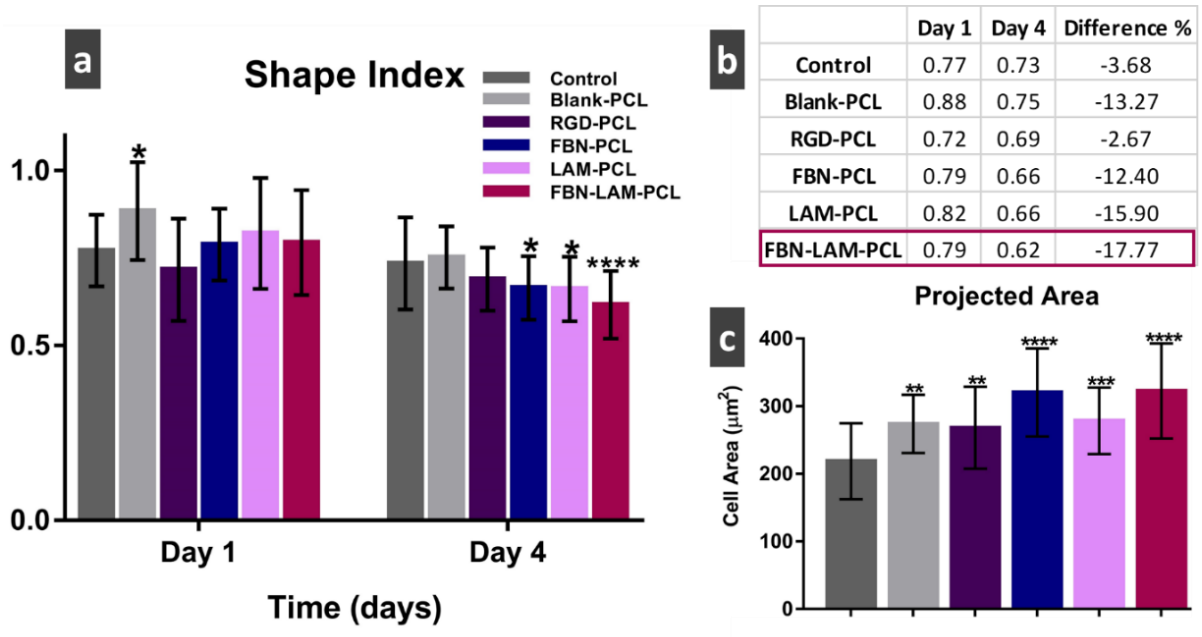

	Day 1	Day 4	Difference %
Control	0.77	0.73	-3.68
Blank-PCL	0.88	0.75	-13.27
RGD-PCL	0.72	0.69	-2.67
FBN-PCL	0.79	0.66	-12.40
LAM-PCL	0.82	0.66	-15.90
FBN-LAM-PCL	0.79	0.62	-17.77

Figure 19. Morphological assessment of neuroblastoma cells grown on different PCL-NFs: (a,b) shape index of cells at day 1 and 4 of the experiment, and (c) total projected area of cells at day 4, both analyzed from light microscope images; One-way ANOVA; *p < 0.05, **p < 0.01, ***p < 0.001, and ****p < 0.0001.

`

5. Conclusion and Future Work

5.1. Conclusion

In the present study, a novel composite nanofibrous scaffold composed of randomly aligned PCL with attached dual FBN and LAM, mimicking the developing central nervous system, was fabricated and compared to other fabricated NFs of either blank PCL or with solely RGD, FBN, or LAM, alone. The chemical grafting was successfully conducted post-spinning, and fabricated NFs exhibited adequate physical stability to accommodate neuronal regeneration purposes. This study highlights the synergistic mechanism of the proposed PCL scaffold with combined LAM and FBN, with demonstrated biocompatibility and potentials for neuronal differentiation of SH-SY5Y cells. This is manifested in a decreased proliferation rate, higher cellular attachment, developed polar morphology of the cells, extended neurite outgrowth and neuronal network connection. The gathered results of this work strongly suggest superior capability of the dual conjugation in guiding neuronal and axonal regeneration. In this context, it may have the potential for promoting regenerative neuronal connectivity in SCI, once tested *in vivo* in suitable models.

5.2. Future Work

The fabricated NFs need further research including:

- Molecular analysis to study the effect of the NFs on the protein and gene expression of cells.
- Comprehensive animal study to evaluate the locomotor activity of treated groups using the fabricated NFs.

`

6. References

1. Heimer, L. *The Human Brain and Spinal Cord Functional Neuroanatomy and Dissection Guide*. (1983).

2. Sabharwal, S. *Essentials of Spinal Cord Medicine.* (Demos Medical Publishing, 2013).

3. *International perspectives on spinal cord injury*. (World Health Organization, 2013).

4. Sekhon, L. H. & Fehlings, M. G. Epidemiology, demographics, and pathophysiology of acute spinal cord injury. *Spine (Phila. Pa. 1976).* **26**, S2-12 (2001).

5. Singh, A., Tetreault, L., Kalsi-Ryan, S., Nouri, A. & Fehlings, M. G. Global prevalence and incidence of traumatic spinal cord injury. *Clin. Epidemiol.* **6**, 309–331 (2014).

6. Hagen, E. M. Acute complications of spinal cord injuries. *World J. Orthop.* **6**, 17–23 (2015).

7. H. Elshahidi, M. *et al.* Epidemiological Characteristics of Traumatic Spinal Cord Injury (TSCI) in the Middle-East and North-Africa (MENA) Region: A Systematic Review and Meta-Analysis. *Bull. Emerg. Trauma* **6**, 75–89 (2018).

8. Rahimi-Movaghar, V. *et al.* Epidemiology of Traumatic Spinal Cord Injury in Developing Countries: A Systematic Review. *Neuroepidemiology* **41**, 65–85 (2013).

9. Ahoniemi, E., Pohjolainen, T. & Kautiainen, H. Survival after spinal cord injury in Finland. *J. Rehabil. Med.* **43**, 481–485 (2011).

10. Nulle, A., Tjurina, U., Erts, R. & Vetra, A. A profile of traumatic spinal cord injury and medical complications in Latvia. *Spinal Cord Ser. Cases* **3**, (2017).

`

11. Obalum, D. C., Giwa, S. O., Adekoya-Cole, T. O. & Enweluzo, G. O. Profile of spinal injuries in Lagos, Nigeria. *Spinal Cord* **47**, 134–137 (2009).

12. McDonald, J. W. & Sadowsky, C. Spinal-cord injury. in *Lancet* **359**, 417–425 (Elsevier Limited, 2002).

13. *Spinal Cord Injury Facts and Figures at a Glance*. (2019).

14. Krueger, H., Rivers, C. S., Trenaman, L. M., Noonan, V. K. & Joshi, P. The Economic Burden of Traumatic Spinal Cord Injury in Canada. *Chronic Dis. Inj. Can.* **33**, (2013).

15. *The economic cost of spinal cord injury and traumatic brain injury in Australia*. (2009).

16. Meerding, W. J., Mulder, S. & van Beeck, E. F. Incidence and costs of injuries in The Netherlands. *Eur. J. Public Health* **16**, 271–277 (2006).

17. Kreydin, E. *et al.* Surveillance and management of urologic complications after spinal cord injury. *World J. Urol.* **36**, 1545–1553 (2018).

18. Haisma, J. *et al.* Complications following spinal cord injury: Occurrence and risk factors in a longitudinal study during and after inpatient rehabilitation. *J. Rehabil. Med.* **39**, 393–398 (2007).

19. Sezer, N., Akkuş, S. & Uğurlu, F. G. Chronic complications of spinal cord injury. *World J. Orthop.* **6**, 24–33 (2015).

20. Li, S. & Stys, P. K. Mechanisms of Ionotropic Glutamate Receptor-Mediated Excitotoxicity in Isolated Spinal Cord White Matter. *J. Neurosci.* **20**, 1190–1198 (2000).

`

21. Xu, G.-Y., Hughes, M. G., Ye, Z., Hulsebosch, C. E. & McAdoo, D. J. Concentrations of glutamate released following spinal cord injury kill oligodendrocytes in the spinal cord. *Exp. Neurol.* **187**, 329–336 (2004).

22. Fawcett, J. W. & Asher, R. A. The glial scar and central nervous system repair. *Brain Res. Bull.* **49**, 377–391 (1999).

23. David, S. & Kroner, A. Repertoire of microglial and macrophage responses after spinal cord injury. *Nat. Rev. Neurosci.* **12**, 388–399 (2011).

24. O'Shea, T. M., Burda, J. E. & Sofroniew, M. V. Cell biology of spinal cord injury and repair. *J. Clin. Invest.* **127**, 3259–3270 (2017).

25. Gensel, J. C. & Zhang, B. Macrophage activation and its role in repair and pathology after spinal cord injury. *Brain Res.* **1619**, 1–11 (2015).

26. Zörner, B. & Schwab, M. E. Anti-Nogo on the go: from animal models to a clinical trial: Zörner & Schwab. *Ann. N. Y. Acad. Sci.* **1198**, E22–E34 (2010).

27. Fehlings, M. G. *et al.* A Clinical Practice Guideline for the Management of Acute Spinal Cord Injury: Introduction, Rationale, and Scope. *Global Spine Journal* **7**, 84S-94S (2017).

28. Wang, D., Ichiyama, R. M., Zhao, R., Andrews, M. R. & Fawcett, J. W. Chondroitinase Combined with Rehabilitation Promotes Recovery of Forelimb Function in Rats with Chronic Spinal Cord Injury. *J. Neurosci.* **31**, 9332–9344 (2011).

29. Hu, H. Z., Granger, N., Pai, S. B., Bellamkonda, R. V & Jeffery, N. D. Therapeutic efficacy

of microtube-embedded chondroitinase ABC in a canine clinical model of spinal cord injury. *Brain* **141**, 1017–1027 (2018).

30. Bradbury, E. J. *et al.* Chondroitinase ABC promotes functional recovery after spinal cord injury. *Nature* **416**, 636 (2002).

31. Moon, L. D. F., Asher, R. A., Rhodes, K. E. & Fawcett, J. W. Regeneration of CNS axons back to their target following treatment of adult rat brain with chondroitinase ABC. *Nat. Neurosci.* **4**, 465–466 (2001).

32. Schwab, M. E. Repairing the Injured Spinal Cord. *Science (80-.).* **295**, 1029–1031 (2002).

33. Hu, H. Phase II Double-blinded Randomized Controlled Clinical Trial of Chondroitinase ABC by Intraspinal Injection for Treatment of Severe Chronic Spinal Cord Injury in 60 Pet Dogs. *Grad. Theses Diss.* (2016). doi:https://doi.org/10.31274/etd-180810-5562

34. Schwab, M. E. & Strittmatter, S. M. Nogo limits neural plasticity and recovery from injury. *Curr. Opin. Neurobiol.* **27**, 53–60 (2014).

35. Geoffroy, C. G. & Zheng, B. Myelin-associated inhibitors in axonal growth after CNS injury. *Curr. Opin. Neurobiol.* **27**, 31–38 (2014).

36. Weinmann, O. *et al.* Intrathecally infused antibodies against Nogo-A penetrate the CNS and downregulate the endogenous neurite growth inhibitor Nogo-A. *Mol. Cell. Neurosci.* **32**, 161–173 (2006).

37. Liebscher, T. *et al.* Nogo-A antibody improves regeneration and locomotion of spinal cord-

injured rats. *Ann. Neurol.* **58**, 706–719 (2005).

38. Müllner, A. *et al.* Lamina-specific restoration of serotonergic projections after Nogo-A antibody treatment of spinal cord injury in rats: Restoration of serotonergic projections after anti-Nogo-A antibody treatment. *Eur. J. Neurosci.* **27**, 326–333 (2008).

39. Wang, X., Baughman, K. W., Basso, D. M. & Strittmatter, S. M. Delayed Nogo receptor therapy improves recovery from spinal cord contusion. *Ann. Neurol.* **60**, 540–549 (2006).

40. Freund, P. *et al.* Anti-Nogo-A antibody treatment promotes recovery of manual dexterity after unilateral cervical lesion in adult primates - re-examination and extension of behavioral data. *Eur. J. Neurosci.* **29**, 983–996 (2009).

41. Acute Safety, Tolerability, Feasibility and Pharmacokinetics of Intrath. Administered ATI355 in Patients With Acute SCI - Full Text View - ClinicalTrials.gov. (2019).

42. Kucher, K. *et al.* First-in-Man Intrathecal Application of Neurite Growth-Promoting Anti-Nogo-A Antibodies in Acute Spinal Cord Injury. *Neurorehabil. Neural Repair* **32**, 578–589 (2018).

43. NISCI - Nogo Inhibition in Spinal Cord Injury - Full Text View - ClinicalTrials.gov. (2019).

44. Gaber, T. & Brown, M. Recent advances in neuromodulation for spinal cord injuries. *Prog. Neurol. Psychiatry* **24**, 4–8 (2020).

45. Schmidt, G. L. The Use of Spinal Cord Stimulation/Neuromodulation in the Management of Chronic Pain. *The Journal of the American Academy of Orthopaedic Surgeons* **27**, e401–

`

e407 (2019).

46. Hofstoetter, U. S., Freundl, B., Binder, H. & Minassian, K. Common neural structures activated by epidural and transcutaneous lumbar spinal cord stimulation: Elicitation of posterior root-muscle reflexes. *PLoS One* **13**, (2018).

47. Wagner, F. B. *et al.* Targeted neurotechnology restores walking in humans with spinal cord injury. *Nature* **563**, 65–93 (2018).

48. van den Brand, R. *et al.* Neuroprosthetic technologies to augment the impact of neurorehabilitation after spinal cord injury. *Annals of Physical and Rehabilitation Medicine* **58**, 232–237 (2015).

49. Ganzer, P. D. *et al.* Closed-loop neuromodulation restores network connectivity and motor control after spinal cord injury. *Elife* **7**, e32058 (2018).

50. Sacral Nerve Stimulation in Improving Bladder After Acute Traumatic Spinal Cord Injury - Full Text View - ClinicalTrials.gov. Available at: https://clinicaltrials.gov/ct2/show/NCT03083366. (Accessed: 15th April 2020)

51. Kirshblum, S. C. *et al.* Spinal Cord Injury Medicine. 3. Rehabilitation Phase After Acute Spinal Cord Injury. *Arch. Phys. Med. Rehabil.* **88**, S62–S70 (2007).

52. Nas, K., Yazmalar, L., Şah, V., Aydin, A. & Öneş, K. Rehabilitation of spinal cord injuries. *World J. Orthop.* **6**, 8–16 (2015).

53. Mazwi, N. L., Adeletti, K. & Hirschberg, R. E. Traumatic Spinal Cord Injury: Recovery,

`

Rehabilitation, and Prognosis. *Curr. Trauma Reports* **1**, 182–192 (2015).

54. Schwab, M. E. Repairing the injured spinal cord. (Viewpoint). *Science (80-.).* **295**, 1029+ (2002).

55. Abbas, W. A., Sharafeldin, I. M., Omar, M. M. & Allam, N. K. Novel mineralized electrospun chitosan/PVA/TiO 2 nanofibrous composites for potential biomedical applications: computational and experimental insights . *Nanoscale Adv.* (2020). doi:10.1039/d0na00042f

56. Elsayed, N. A., Zada, S. & Allam, N. K. Mineralization of electrospun gelatin/CaCO 3 composites: A new approach for dental applications. *Mater. Sci. Eng. C* **100**, 655–664 (2019).

57. Qing, H. *et al.* Heterostructured Silk-Nanofiber-Reduced Graphene Oxide Composite Scaffold for SH-SY5Y Cell Alignment and Differentiation. *ACS Appl. Mater. Interfaces* **10**, 39228–39237 (2018).

58. The INSPIRE Study: Probable Benefit of the Neuro-Spinal Scaffold for Treatment of AIS A Thoracic Acute Spinal Cord Injury - Full Text View - ClinicalTrials.gov. Available at: https://clinicaltrials.gov/ct2/show/NCT02138110. (Accessed: 11th May 2020)

59. Study of Probable Benefit of the Neuro-Spinal Scaffold^{TM} in Subjects With Complete Thoracic AIS A Spinal Cord Injury as Compared to Standard of Care - Full Text View - ClinicalTrials.gov. Available at: https://clinicaltrials.gov/ct2/show/NCT03762655. (Accessed: 11th May 2020)

`

60. Functional Neural Regeneration Collagen Scaffold Transplantation in Acute Spinal Cord Injury Patients - Full Text View - ClinicalTrials.gov. Available at: https://clinicaltrials.gov/ct2/show/NCT02510365. (Accessed: 12th May 2020)

61. Functional Scaffold Transplantation Combined With Epidural Electrical Stimulation for Spinal Cord Injury Repair - Full Text View - ClinicalTrials.gov. Available at: https://clinicaltrials.gov/ct2/show/NCT03966794. (Accessed: 12th May 2020)

62. Lukáš, D. *et al.* Physical principles of electrospinning (electrospinning as a nano-scale technology of the twenty-first century). *Text. Prog.* **41**, 59–140 (2009).

63. Ding, J. *et al.* Electrospun polymer biomaterials. *Prog. Polym. Sci.* **90**, 1–34 (2019).

64. Ibrahim, D. M., Kakarougkas, A. & Allam, N. K. Recent advances on electrospun scaffolds as matrices for tissue-engineered heart valves. *Materials Today Chemistry* **5**, 11–23 (2017).

65. (nanofibers) AND (tissue regeneration) - Search Results - PubMed. Available at: https://pubmed.ncbi.nlm.nih.gov/?term=%28nanofibers%29+AND+%28tissue+regeneration%29&sort=. (Accessed: 26th May 2020)

66. Sell, S. A. *et al.* The use of natural polymers in tissue engineering: A focus on electrospun extracellular matrix analogues. *Polymers* **2**, 522–553 (2010).

67. Wrobel, M. R. & Sundararaghavan, H. G. Directed Migration in Neural Tissue Engineering. *Tissue Eng. Part B Rev.* **20**, 93–105 (2014).

68. Marin, E., Boschetto, F. & Pezzotti, G. Biomaterials and biocompatibility: an historical

`

overview. *J. Biomed. Mater. Res. Part A* (2020). doi:10.1002/jbm.a.36930

69. Joosten, E. A. J. Biodegradable biomatrices and bridging the injured spinal cord: The corticospinal tract as a proof of principle. *Cell and Tissue Research* **349**, 375–395 (2012).

70. Faccendini, A. *et al.* Nanofiber scaffolds as drug delivery systems to bridge spinal cord injury. *Pharmaceuticals* **10**, 1–30 (2017).

71. Mitragotri, S. & Lahann, J. Physical approaches to biomaterial design. *Nat. Mater.* **8**, 15–23 (2009).

72. Nguyen, L. H. *et al.* Three-dimensional aligned nanofibers-hydrogel scaffold for controlled non-viral drug/gene delivery to direct axon regeneration in spinal cord injury treatment. *Sci. Rep.* **7**, 1–12 (2017).

73. Maitz, M. F. Applications of synthetic polymers in clinical medicine. *Biosurface and Biotribology* **1**, 161–176 (2015).

74. Tang, X. *et al.* Polymeric Biomaterials in Tissue Engineering and Regenerative Medicine. in *Natural and Synthetic Biomedical Polymers* 351–371 (Elsevier Inc., 2014). doi:10.1016/B978-0-12-396983-5.00022-3

75. Suwantong, O. Biomedical applications of electrospun polycaprolactone fiber mats. *Polym. Adv. Technol.* **27**, 1264–1273 (2016).

76. Janmohammadi, M. & Nourbakhsh, M. S. Electrospun polycaprolactone scaffolds for tissue engineering: a review. *Int. J. Polym. Mater. Polym. Biomater.* **68**, 527–539 (2019).

`

77. Mochane, M. J., Motsoeneng, T. S., Sadiku, E. R., Mokhena, T. C. & Sefadi, J. S. Morphology and properties of electrospun PCL and its composites for medical applications: A mini review. *Appl. Sci.* **9**, 1–17 (2019).

78. Heimowska, A., Morawska, M. & Bocho-Janiszewska, A. Biodegradation of poly(ϵ-caprolactone) in natural water environments. *Polish J. Chem. Technol.* **19**, 120–126 (2017).

79. Zhou, X. *et al.* Polycaprolactone electrospun fiber scaffold loaded with iPSCs-NSCs and ASCs as a novel tissue engineering scaffold for the treatment of spinal cord injury. *Int. J. Nanomedicine* **Volume 13**, 6265–6277 (2018).

80. Zhang, S. *et al.* Polycaprolactone/polysialic acid hybrid, multifunctional nanofiber scaffolds for treatment of spinal cord injury. *Acta Biomater.* **77**, 15–27 (2018).

81. Neal, R. A. *et al.* Alignment and composition of laminin-polycaprolactone nanofiber blends enhance peripheral nerve regeneration. *J Biomed Mater Res A* **100**, 406–423 (2012).

82. Prabhakaran, M. P., Venugopal, J., Chan, C. K. & Ramakrishna, S. Surface modified electrospun nanofibrous scaffolds for nerve tissue engineering. *Nanotechnology* **19**, 455102 (2008).

83. Song, J. *et al.* The preparation and characterization of polycaprolactone/graphene oxide biocomposite nanofiber scaffolds and their application for directing cell behaviors. *Carbon N. Y.* **95**, 1039–1050 (2015).

84. Junka, R., Valmikinathan, C. M., Kalyon, D. M. & Yu, X. Laminin Functionalized Biomimetic Nanofibers For Nerve Tissue Engineering. doi:10.1166/jbt.2013.1110

`

85. Zamani, F., Amani-Tehran, M., Zaminy, A. & Shokrgozar, M. A. Conductive 3D structure nanofibrous scaffolds for spinal cord regeneration. *Fibers Polym.* **18**, 1874–1881 (2017).

86. Zhou, X. *et al.* Polycaprolactone electrospun fiber scaffold loaded with iPSCs-NSCs and ASCs as a novel tissue engineering scaffold for the treatment of spinal cord injury. *Int. J. Nanomedicine* **Volume 13**, 6265–6277 (2018).

87. Schnell, E. *et al.* Guidance of glial cell migration and axonal growth on electrospun nanofibers of poly-ε-caprolactone and a collagen/poly-ε-caprolactone blend. *Biomaterials* **28**, 3012–3025 (2007).

88. Ghasemi-Mobarakeh, L., Prabhakaran, M. P., Morshed, M., Nasr-Esfahani, M. H. & Ramakrishna, S. Electrospun poly(ε-caprolactone)/gelatin nanofibrous scaffolds for nerve tissue engineering. *Biomaterials* **29**, 4532–4539 (2008).

89. Gerardo-Nava, J. *et al.* Human neural cell interactions with orientated electrospun nanofibers in vitro. *Nanomedicine* **4**, 11–30 (2009).

90. Subramanian, A., Krishnan, U. M. & Sethuraman, S. Fabrication, characterization and in vitro evaluation of aligned PLGA-PCL nanofibers for neural regeneration. *Ann. Biomed. Eng.* **40**, 2098–2110 (2012).

91. Liverani, L., Killian, M. S. & Boccaccini, A. R. Fibronectin functionalized electrospun fibers by using benign solvents: Best way to achieve effective functionalization. *Front. Bioeng. Biotechnol.* **7**, 1–12 (2019).

92. Grinnell, F. & Feld, M. K. *Fibronectin Adsorption on Hydrophilic and Hydrophobic*

`

Surfaces Detected by Antibody Binding and Analyzed during Cell Adhesion in Serum-containing Medium. THE JOURNAL OF BIOLOGICAI. CHEMISTRY* **257**, (1982).

93. Kohno, U. S. A. *et al. Laminin, a Multidomain Protein THE A CHAIN HAS A UNIQUE GLOBULAR DOMAIN AND HOMOLOGY WITH THE BASEMENT MEMBRANE PROTEOGLYCAN AND THE LAMININ B CHAINS*. THE JOURNAL OF BIOLOGICAL CHEMISTRY* **263**, (1988).

94. Bellis, S. L. Advantages of RGD peptides for directing cell association with biomaterials. *Biomaterials* **32**, 4205–4210 (2011).

95. Equipment NANON-01A | Mecc Corporation. Available at: https://www.mecc-nano.com/equipment03.html. (Accessed: 12th May 2020)

96. Chong, E. J. *et al.* Evaluation of electrospun PCL/gelatin nanofibrous scaffold for wound healing and layered dermal reconstitution. *Acta Biomater.* **3**, 321–330 (2007).

97. Papouin, T. & Haydon, P. Obtaining Acute Brain Slices. *BIO-PROTOCOL* **8**, (2018).

98. Ciapetti, G., Cenni, E., Pratelli, L. & Pizzoferrato, A. In vitro evaluation of cell/biomaterial interaction by MTT assay. *Biomaterials* **14**, 359–364 (1993).

99. Wang, D., Jang, J., Kim, K., Kim, J. & Park, C. B. 'tree to Bone': Lignin/Polycaprolactone Nanofibers for Hydroxyapatite Biomineralization. *Biomacromolecules* **20**, 2684–2693 (2019).

100. Bongiovanni Abel, S., Liverani, L., Boccaccini, A. R. & Abraham, G. A. Effect of benign

`

solvents composition on poly(ε-caprolactone) electrospun fiber properties. *Mater. Lett.* **245**, 86–89 (2019).

101. Matsumoto, H. & Tanioka, A. Functionality in electrospun nanofibrous membranes based on fiber's size, surface area, and molecular orientation. *Membranes (Basel).* **1**, 249–264 (2011).

102. Cammarata, C. R., Hughes, M. E. & Ofner, C. M. Carbodiimide induced cross-linking, ligand addition, and degradation in gelatin. *Mol. Pharm.* **12**, 783–793 (2015).

103. Carbodiimide Crosslinker Chemistry | Thermo Fisher Scientific - EG. Available at: https://www.thermofisher.com/eg/en/home/life-science/protein-biology/protein-biology-learning-center/protein-biology-resource-library/pierce-protein-methods/carbodiimide-crosslinker-chemistry.html. (Accessed: 12th May 2020)

104. Khan, M. S. I., Oh, S. W. & Kim, Y. J. Power of Scanning Electron Microscopy and Energy Dispersive X-Ray Analysis in Rapid Microbial Detection and Identification at the Single Cell Level. *Sci. Rep.* **10**, 1–10 (2020).

105. Guler, Z., Silva, J. C. & Sezai Sarac, A. RGD functionalized poly(ε-caprolactone)/poly(m-anthranilic acid) electrospun nanofibers as high-performing scaffolds for bone tissue engineering RGD functionalized PCL/P3ANA nanofibers. *Int. J. Polym. Mater. Polym. Biomater.* **66**, 139–148 (2017).

106. Selvam, N. C. S., Kumar, R. T., Kennedy, L. J. & Vijaya, J. J. Comparative study of microwave and conventional methods for the preparation and optical properties of novel

`

MgO-micro and nano-structures. *J. Alloys Compd.* **509**, 9809–9815 (2011).

107. Barth, A. Infrared spectroscopy of proteins. *Biochimica et Biophysica Acta - Bioenergetics* **1767**, 1073–1101 (2007).

108. Zhao, J. & Wang, J. Uncovering the Sensitivity of Amide-II Vibration to Peptide-Ion Interactions. *J. Phys. Chem. B* **120**, 9590–9598 (2016).

109. Augustine, R., Thomas, S. & Kalarikkal, N. In Vitro Degradation of Electrospun Polycaprolactone Membranes in Simulated Body Fluid. *Int. J. Inst. Mater. Malaysia* **2**, 211–220 (2014).

110. Valenzuela, L. M., Michniak, B. & Kohn, J. Variability of water uptake studies of biomedical polymers. *J. Appl. Polym. Sci.* **121**, 1311–1320 (2011).

111. Zahedi, P., Rezaeian, I., Jafari, S. H. & Karami, Z. Preparation and release properties of electrospun poly(vinyl alcohol)/poly(É-caprolactone) hybrid nanofibers: Optimization of process parameters via D-optimal design method. *Macromol. Res.* **21**, 649–659 (2013).

112. Mondal, D., Griffith, M. & Venkatraman, S. S. Polycaprolactone-based biomaterials for tissue engineering and drug delivery: Current scenario and challenges. *International Journal of Polymeric Materials and Polymeric Biomaterials* **65**, 255–265 (2016).

113. dos Santos, D. M. *et al.* Nanostructured electrospun nonwovens of poly(ε-caprolactone)/quaternized chitosan for potential biomedical applications. *Carbohydr. Polym.* **186**, 110–121 (2018).

`

114. Head, D. A., Levine, A. J. & Mackintosh, F. C. Deformation of Cross-Linked Semiflexible Polymer Networks. doi:10.1103/PhysRevLett.91.108102

115. Moeendarbary, E. *et al.* The soft mechanical signature of glial scars in the central nervous system. *Nat. Commun.* **8**, 1–11 (2017).

116. Rodríguez Hernández, J. C., Sánchez, M. S., Soria, J. M., Gómez Ribelles, J. L. & Pradas, M. M. Substrate chemistry-dependent conformations of single laminin molecules on polymer surfaces are revealed by the phase signal of atomic force microscopy. *Biophys. J.* **93**, 202–207 (2007).

117. Dwane, S., Durack, E. & Kiely, P. A. Optimising parameters for the differentiation of SH-SY5Y cells to study cell adhesion and cell migration. *BMC Res. Notes* **6**, 366 (2013).

118. Kovalevich, J. & Langford, D. Considerations for the use of SH-SY5Y neuroblastoma cells in neurobiology. *Methods Mol. Biol.* **1078**, 9–21 (2013).

119. Zhou, H., Weir, M. D. & Xu, H. H. K. Effect of cell seeding density on proliferation and osteodifferentiation of umbilical cord stem cells on calcium phosphate cement-fiber scaffold. *Tissue Eng. - Part A* **17**, 2603–2613 (2011).

120. Wong, D. Y. *et al.* Macro-architectures in spinal cord scaffold implants influence regeneration. *J. Neurotrauma* **25**, 1027–1037 (2008).

121. Teppola, H., Sarkanen, J. R., Jalonen, T. O. & Linne, M. L. Morphological Differentiation Towards Neuronal Phenotype of SH-SY5Y Neuroblastoma Cells by Estradiol, Retinoic Acid and Cholesterol. *Neurochem. Res.* **41**, 731–747 (2016).

`

122. Murtey, M. Das & Ramasamy, P. Sample Preparations for Scanning Electron Microscopy – Life Sciences. in *Modern Electron Microscopy in Physical and Life Sciences* (InTech, 2016). doi:10.5772/61720

123. Braet, F., De Zanger, R. & Wisse, E. Drying cells for SEM, AFM and TEM by hexamethyldisilazane: a study on hepatic endothelial cells. *J. Microsc.* **186**, 84–87 (1997).

124. Lowery, L. A. & Vactor, D. Van. The trip of the tip: Understanding the growth cone machinery. *Nature Reviews Molecular Cell Biology* **10**, 332–343 (2009).

125. Salmerón-Sánchez, M. & Dalby, M. J. Synergistic growth factor microenvironments. *Chemical Communications* **52**, 13327–13336 (2016).

126. De Franceschi, N. *et al.* ProLIF – Quantitative integrin protein–protein interactions and synergistic membrane effects on proteoliposomes. *J. Cell Sci.* **132**, (2019).

127. Wang, W. *et al.* Enhancing the hydrophilicity and cell attachment of 3D printed PCL/graphene scaffolds for bone tissue engineering. *Materials (Basel).* **9**, (2016).

7. Appendix

Phosphate Buffer. Prepare a 0.2M phosphate buffer of pH 7.2 as follows: add 10.22 g Na_2HPO_4 and 3.36 g NaH_2PO_4 to deionized water to a final volume of 500 ml. Dilute to obtain other concentrations as needed.

McDowell and Trump's Fixative (1976). This fixative contains 4% formaldehyde and 1% glutaraldehyde in 0.1M phosphate buffer. Use 50 ml of 0.2M phosphate buffer, add 11 ml of 37% formaldehyde solution, add 4 ml of a 25% glutaraldehyde solution, then add distilled water to a final volume of 100 ml.

Ethanol Dehydration. NFs samples are washed and immersed in the McDowell and Trump's fixative solution for 30 mins in room temperature. Following, samples are washed with phosphate buffer, two times for 10 mins each, then with deionized water one time for 10 mins. After this, samples are dehydrated in the following order, 15 mins each (35%, 50%, 75%, absolute ethanol). Finally, NFs left to dry overnight in a 15 cm desiccator.